

Phase Transitions with imaginary chemical potential in the PNJL model

Bachelor thesis by Constantin Sporleder

Date of submission: March 16, 2021

1. Review: PD. Dr. Michael Buballa

2. Review: Prof. Dr. Guy Moore

Darmstadt



TECHNISCHE
UNIVERSITÄT
DARMSTADT

Physik
Institut für Kernphysik
Theoriezentrum
NHQ-Gruppe

Erklärung zur Abschlussarbeit gemäß §22 Abs. 7 und §23 Abs. 7 APB der TU Darmstadt


Hiermit versichere ich, Constantin Sporleder, die vorliegende Bachelorarbeit ohne Hilfe Dritter und nur mit den angegebenen Quellen und Hilfsmitteln angefertigt zu haben. Alle Stellen, die Quellen entnommen wurden, sind als solche kenntlich gemacht worden. Diese Arbeit hat in gleicher oder ähnlicher Form noch keiner Prüfungsbehörde vorgelegen.

Mir ist bekannt, dass im Fall eines Plagiats (§38 Abs. 2 APB) ein Täuschungsversuch vorliegt, der dazu führt, dass die Arbeit mit 5,0 bewertet und damit ein Prüfungsversuch verbraucht wird. Abschlussarbeiten dürfen nur einmal wiederholt werden.

Bei der abgegebenen Thesis stimmen die schriftliche und die zur Archivierung eingereichte elektronische Fassung gemäß §23 Abs. 7 APB überein.

Bei einer Thesis des Fachbereichs Architektur entspricht die eingereichte elektronische Fassung dem vorgestellten Modell und den vorgelegten Plänen.

Darmstadt, 16. März 2021


C. Sporleder

Abstract

In this work, the phase diagram of QCD will be investigated using the NJL model and the PNJL model for two quark flavors in the limit of identical quark masses. This will be done for real and imaginary chemical potentials. With these models, the phase transition lines of the chiral phase transition and the confinement/deconfinement phase transition. The chiral susceptibilities will also be calculated and will serve as a transition criterion for the chiral phase transition. The results will be compared to the results of lattice QCD.

Contents

1	Physical Principles	8
1.1	Principles of QCD	8
1.1.1	Lagrangian of QCD	8
1.1.2	Symmetries of QCD	9
1.1.3	The QCD Phase Diagram	10
1.1.4	Lattice QCD	11
1.1.5	Lattice QCD at imaginary chemical Potential	12
1.2	The Nambu-Jona-Lasinio Model	12
1.2.1	Lagrangian of the NJL Model	13
1.2.2	Symmetries of the NJL Model	13
1.2.3	Constituent quark mass	15
1.2.4	Mean-field Approximation	18
1.2.5	Thermodynamic Potential	19
1.2.6	Parameters	21
1.2.7	Imaginary chemical potential	21
1.2.8	Phase Transitions	22
1.3	The PNJL Model	23
1.3.1	The Polyakov-Loop	23
1.3.2	Lagrangian of the PNJL model	24
1.3.3	The Thermodynamic Potential	26
1.3.4	Imaginary chemical potential	27
1.3.5	Phase transitions	29
2	Phase Transitions in the NJL model	31
2.1	Solving the gap equation at real chemical potential	31
2.1.1	The NJL phase diagram at real chemical potential	33
2.2	Solving the gap equation at imaginary chemical potential	33
2.2.1	The NJL Phase diagram at imaginary chemical potential	34

3	Phase Transitions in the PNJL model	38
3.1	Solving the gap equation at real chemical potential	38
3.1.1	The PNJL phase diagram at real chemical potential	40
3.2	Solving the gap equation at imaginary chemical potential	41
3.2.1	The PNJL phase diagram at imaginary chemical potential	42
4	Comparisons with Lattice QCD	45
5	Conclusion and Outlook	49
6	Appendix	53

Motivation

"In the beginning the universe was created. This has made a lot of people very angry and has been widely regarded as a bad move."

Douglas Adams

In the early universe, just microseconds after the Big Bang, matter was under extreme conditions. Under these extreme conditions, quarks and gluons became free and deconfined and formed a quark-gluon plasma. In this state, quarks and gluons can move unbound. It is also possible, that the deconfined state is also present in rather cold, but highly dense neutron stars. This state stands in high contrast to the state of the rest of the observable universe, where quarks can only be observed in colorless compounds [1]. It is therefore of great interest to study the phase structure of quantum chromodynamics, which is the theory of strong interaction and therefore the interaction between quarks and gluons.

Those extreme conditions are also achieved with high energy collisions in the Large hadron collider (LHC) at CERN.

In this work, we will investigate the phase diagram of QCD. Specifically, we will calculate the phase transition lines of the chiral phase transition and the phase transitions to the deconfined phase. For that, we will use the NJL model and its extension, the PNJL model. Both are used as effective quark models. The NJL model is, although in its beginning intended to be a model to describe nucleons, a popular effective quark model, since it contains similar symmetries as QCD, such as the nearly exact chiral symmetry. However, it does not contain confinement [2]. That is why we will also consider the PNJL model, which takes confinement into account in the form of the Polyakov loop. To further simplify

calculations, we will consider the limes of identical quark masses for two flavors.

The phase transition in this work is interpreted as a change in the respective order parameters. Those are the chiral condensate, in the NJL model expressed as the constituent quark mass, for the chiral phase transition and the Polyakov loop expectation value for the confinement to deconfinement transition. We expect to find chiral crossover transitions at high temperatures and chiral first order transitions for high chemical potentials. It is also expected to find a critical point, where those turn into each other. This will also be determined in this work. As a transition criterion will be chosen a peak in the respective susceptibility.

With the help of those models, we can conduct calculations at nonzero chemical potential, which is fairly difficult to do with lattice QCD. A possibility to deal with this problem is to switch to imaginary chemical potential. Although there is no physical interpretation of an imaginary potential, calculations become possible. Then we can extrapolate those results to real chemical potential. In this work, we will also compare the results of lattice QCD at imaginary potential with those conducted in the PNJL model. The lattice QCD results will be taken from [3]. This is hoped to give this model validation and affirm its results in the realm of real chemical potentials.

This work is closely related to the former work [4], where phase transitions at imaginary potential in the NJL and PNJL were conducted. In this work, additionally, the chiral susceptibilities were calculated. Further, the results are compared to newly achieved lattice QCD results.

In this work, all quantities will be expressed in natural units. This means

$$\hbar = c = k_B = 1.$$

1 Physical Principles

1.1 Principles of QCD

Here, the basic principles of quantum chromodynamics shall be reviewed briefly. A more detailed discussion can i.e. be found in refs. [5], [1].

Quantum chromodynamics (QCD) is the theory of strong interaction, which describes the interaction of quarks and gluons. Those particles are the constituents of hadrons and mesons. Quarks are assumed to be point-like elementary particles with a spin of $\frac{1}{2}$ and an electric charge of $-\frac{1}{3}e$ and $\frac{2}{3}e$. There have been six quark flavors discovered: up (u), down (d), strange (s), charm (c), top (t) and bottom (b). Furthermore, quarks can only be observed in $q\bar{q}$ and qqq systems. Some particles, such as the Δ^{++} particle, which consists of three up quarks and has a spin of $\frac{3}{2}$, seemed to violate the Pauli principle, which states, that each state can only be occupied by one particle. This led to the principle of color charges, which denotes a new quantum number. Each quark and gluon carries a color charge, which can either be green (G), red (R), or blue (B) or its respective anti-color. Observations suggest, that a system can only exist in SU(3) singlets. There can be no unbound, free quarks. This phenomenon is called "confinement" [6].

1.1.1 Lagrangian of QCD

The Lagrangian of QCD is defined by [6]

$$\mathcal{L}_{QCD} = \bar{\psi}(i\gamma^\mu D_\mu - \hat{m})\psi - \frac{1}{4}G^{a\mu\nu}G_{\mu\nu}^a. \quad (1.1)$$

ψ is a quark field, consisting of the six flavors (u, d, s, c, t, b) and three colors (R, G, B). The mass matrix \hat{m} is defined as $\hat{m} = \text{diag}_f(m_u, m_d, \dots)$. The covariant derivative is

$$D_\mu = \partial_\mu - ig \frac{\lambda^a}{2} A_\mu^a \quad (1.2)$$

with the gluon field A_μ^a . The gluon field strength tensor is defined as

$$G_{\mu\nu}^a = \partial_\mu A_\nu^a - \partial_\nu A_\mu^a + gf^{abc} A_\mu^b A_\nu^c. \quad (1.3)$$

The matrices λ^a denote the eight generators of the SU(3) space, namely the Gell-Mann matrices while f^{abc} denote the antisymmetric structure factors. the constant g denotes the coupling constant of QCD. The Lagrangian contains couplings of gluons and quarks, as well as gluonic self couplings (three and four point interactions), which are not present in abelian gauge theories.

Furthermore, the coupling of QCD becomes weak at short distances or low euclidean momenta. This phenomenon is referred to as " asymptotic freedom" [1].

1.1.2 Symmetries of QCD

Quantum chromodynamics is a local non-abelian gauge theory. It is by construction invariant under SU(3) transformations in color space. These transformations can be written as

$$\psi \rightarrow \exp\left(i\frac{g}{2}\lambda^a\Theta_a\right)\psi. \quad (1.4)$$

Here, λ^a again denotes the generators of the strong interaction or Gell-Mann matrices and $\Theta_a = \Theta_a(x)$ are eight local independent transformation "angles".

Furthermore, \mathcal{L}_{QCD} is approximately invariant under SU(N_f) transformations in the flavor space. These are equivalent to global vector- and axialvector transformations

$$\begin{aligned} \psi &\rightarrow \exp(i\Theta_a^V \tau_a)\psi \\ \psi &\rightarrow \exp(i\Theta_a^A \gamma_5 \tau_a)\psi. \end{aligned} \quad (1.5)$$

This chiral symmetry would be exact for massless flavors (chiral limes). However, this is still a good approximation for light flavors, such as up and down. It does not hold, if heavier quarks, such as top and bottom are considered. In the ground state however, the chiral symmetry is absent and therefore spontaneously broken [1]. However, it is restored at high temperatures and high chemical potentials.

1.1.3 The QCD Phase Diagram

Since experimental results and theoretical predictions on the behaviour of quark matter are limited, the exact phase boundaries of the QCD phase diagram are still not very well known [2]. The phase diagram is often presented in the $T - \mu$ -plane, where T denotes the temperature and μ the quark chemical potential. Often, literature refers to the Baryo-chemical potential $\mu_B = 3\mu$, which denotes the chemical potential of a baryon. A sketch of the phase diagram can be seen in fig. 1.1. However, due to various flavors, there are several chemical potentials, each for every flavor, which can produce different phase diagrams. In this work, only one chemical potential will be considered, since we will focus on identical quark masses for two flavors. Furthermore, we will take a look at the phase transition from the hadronic phase to the "deconfined" phase, where quarks and gluons become "deconfined" and can exist freely. This state is expected, when the density of hadronic matter becomes so high, that hadrons physically overlap. This is expected to happen at high temperatures and high chemical potentials [7].

There are various states of strongly interacting matter.

- In the hadronic, confined phase there are different states, such as nuclear matter, a hadronic liquid at high chemical potentials and low temperature and a hadron gas at higher temperature [2].
- The Quark Gluon Plasma (QGP) in the deconfined phase. In this state, the physical degrees of freedom are quarks and gluons.
- Another possible state is a color superconductor phase at low temperatures and high chemical potential. In this state, attractive interaction leads to the formation of bound bosonic diquark pairs. This state can be seen as an analogy to a superconductor in BCS theory.

The QGP might exist inside neutron stars, remains of supernovae with high density. There are also experiments with ultra-heavy ion collisions, which try to produce the densities needed for those states [7].

If a phase transition occurs, one also expects a change in the effective constituent quark mass. In the "confined" phase, quarks are bound inside hadrons. The "bare" quark mass $m_q \approx 0$ is therefore replaced by a much higher constituent quark mass, which takes its

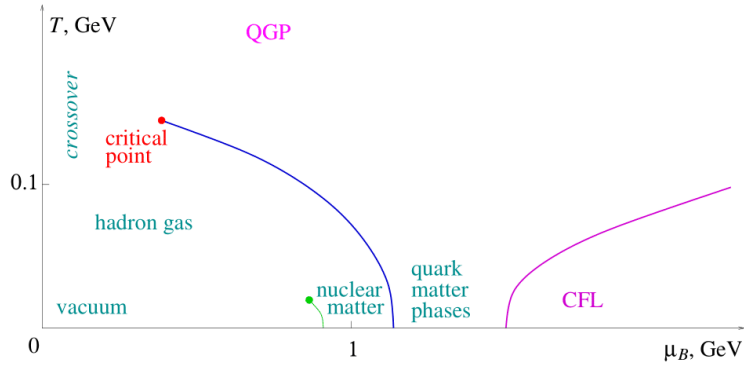


Figure 1.1: The QCD phase-Diagram in the $T - \mu_B$ -plain, taken from ref. [8]. CFL denotes a color superconductor state. At the critical point, the first order chiral phase transition (blue line), turns into a crossover transition.

binding energy into consideration [7].

There are various methods to determine the boundaries of the phase diagram. Most prominent are ab-initio Monte Carlo calculations. Those were restricted to the $\mu = 0$ case for a long time, since the fermion determinant of the QCD partition function turns complex for non-zero chemical potentials. One possibility to avoid this problem is to determine the Taylor coefficients at $\mu = 0$ and extrapolate via a Taylor expansion in terms of $\frac{\mu}{T}$. Another option is to extrapolate results from imaginary chemical potential, since there the fermion determinant stays real. Another option, which also will be used in this work, is to use simplified models of QCD, such as NJL-type models, which also deliver results for non vanishing chemical potentials [2].

1.1.4 Lattice QCD

The basic idea of Lattice QCD is to discretize space time on a lattice. This Lattice can i.e. hypercubic equally spaced lattice of the form

$$x_\mu \rightarrow x(i, j, k, l) = (i\vec{e}_1 + j\vec{e}_2 + k\vec{e}_3 + l\vec{e}_4)a. \quad (1.6)$$

Here a denotes the distance between neighbouring lattice points. Calculating observables on this lattice can i.e. be done using the path integral method. A detailed approach can be found in [1].

1.1.5 Lattice QCD at imaginary chemical Potential

As mentioned above, direct lattice QCD becomes impossible at nonzero chemical potential, since there the fermion determinant becomes imaginary. One method to solve this problem is to examine the solutions at imaginary chemical potential, since there, lattice QCD becomes solvable. Then the solutions can be extrapolated to real chemical potential. However, detailed results for high chemical potentials face great difficulties, since extrapolations tend to get inaccurate outside the vicinity of $\mu = 0$. One method is calculating the Taylor coefficients of the crossover temperature. This can be parametrized as

$$\frac{T_c(\mu)}{T_c(\mu=0)} = 1 - \kappa_2 \left(\frac{\mu}{T_c(\mu)} \right)^2 - \kappa_4 \left(\frac{\mu}{T_c(\mu)} \right)^4. \quad (1.7)$$

Here, $T_c(\mu)$ denotes the crossover temperature at the chemical potential μ . κ_2 and κ_4 are the respective Taylor coefficients. This was i.e. done in [3].

1.2 The Nambu-Jona-Lasinio Model

The NJL-model, originally developed by Nambu and Jona-Lasinio, was created in 1961, before the development of QCD. Its original idea was to describe the interaction of nucleons and had no connection to the description of quarks and gluons. The basic idea was to explain the masses of Dirac particles in analogy to the energy gap in the superconductor BCS theory. In BCS theory, there is an energy gap between holes and electrons in a conductor. This energy gap is due to phonon interaction, which creates correlated electron pairs. To break this correlation, the gap energy must be expended. The interaction of Dirac particles can be described in analogy to the phonon interaction, which yields the basic idea for the NJL model. Further information can be found in [9]. The NJL model does not contain confinement or the interactions of gluons. However, it does contain important global symmetries of QCD, such as the chiral symmetry and is therefore used as an effective model for the interactions of quarks. As noted, the chiral symmetry is just

a real symmetry for vanishing quark masses. This symmetry is spontaneously broken in vacuum. As a result, the pion emerges as the corresponding Goldstone boson to the spontaneously broken chiral symmetry [2]. In the following, we will focus on a two-flavor model ($N_f = 2$) in the isospin-limes, which is the limes of equal quark masses ($m_u = m_d$).

1.2.1 Lagrangian of the NJL Model

The Lagrangian of the NJL for two flavors is [2]

$$\mathcal{L}_{NJL} = \bar{\psi}(i\cancel{\partial} - \hat{m})\psi + g[(\bar{\psi}\psi)^2 + (\bar{\psi}i\gamma_5\vec{\tau}\psi)^2]. \quad (1.8)$$

Here, ψ denotes the quark field, g the coupling constant and $\vec{\tau}$ the vector of the Pauli-matrices in isospin space.

In the case of equal quark masses ($m_u = m_d$), $\hat{m} = \text{diag}(m_u, m_d)$ becomes $\hat{m} = m\mathbb{1}$.

This Lagrangian contains the free Dirac-part

$$\mathcal{L}_{free} = \bar{\psi}(i\cancel{\partial} - \hat{m})\psi, \quad (1.9)$$

which can also be found in the QCD Lagrangian (eq. (1.1)) and denotes the Lagrangian of a free particle. The interaction part

$$\mathcal{L}_{int} = g[(\bar{\psi}\psi)^2 + (\bar{\psi}i\gamma_5\vec{\tau}\psi)^2] \quad (1.10)$$

describes the quark interaction. The quarks here interact via pointlike, four-point vertices [2]. NJL model types have proved to be an effective tool to describe certain aspects of the strong interaction. However, it does not contain gluons. Also, it does not contain the $Z(3)$ center symmetry, which is present in QCD. Later we will discuss the PNJL model, which extends the NJL model by adding a description of gluons and also contains the $Z(3)$ symmetry.

1.2.2 Symmetries of the NJL Model

As mentions above, the NJL-model features similar symmetries as QCD. The NJL-Lagrangian (1.8) for two flavors ($N_f = 2$) is invariant under $U_V(1)$ -transformations.

$$\psi \rightarrow \exp(-i\alpha)\psi. \quad (1.11)$$



Figure 1.2: A sketch to illustrate the Dyson equation. The thick line denotes the propagator of the constituent quark mass, while the thin line denotes the propagator of the bare quark mass.

Here, α denotes an arbitrary rotation angle. This invariance guarantees the baryon number conservation and can simply be shown [10].

A further invariance is the invariance under $SU_V(2)$ transformations in the flavour space

$$\psi \rightarrow \exp\left(-i\vec{\tau}\frac{\vec{\Theta}}{2}\right)\psi. \quad (1.12)$$

Here, $\vec{\Theta} \in \mathbb{R}^3$ denotes a rotation vector. This transformation causes a rotation in the flavor space. Hence, it is only exact in the isospin lines of identical quark masses. This invariance can be shown directly for infinitesimal rotations [10].

Additionally, in the chiral limit ($m_u = m_d = 0$), the Lagrangian is also invariant under $SU_A(2)$ axial vector transformations [10],

$$\psi \rightarrow \exp\left(-i\gamma_5\vec{\tau}\frac{\vec{\Theta}}{2}\right)\psi. \quad (1.13)$$

As in QCD, the chiral symmetry is spontaneously broken in vacuum and restored at high temperatures and chemical potential. By the Goldstone theorem, as a consequence, this requires the existence of a Goldstone boson. The associated particle in this case could be identified as the pion [2].

1.2.3 Constituent quark mass

The self-energy of interaction in the NJL model increases the effective mass of the quarks. This constituent quark mass M can be considerably higher than the bare quark mass. M can be calculated via the Dyson-equation, depicted in figure 1.2. Since the self-energy is, by assumption, local, it can be expressed via a constant shift Σ of the bare quark mass m .

$$M = m + \Sigma \quad (1.14)$$

To calculate it, the Hartree-approximation is used. Therefore, we use the Dirac propagator for fermions in Hartree-approximation. The free quark propagator is given by

$$S_m(p) = \frac{\not{p} + m}{p^2 - m^2 + i\epsilon}. \quad (1.15)$$

The quark propagator for the constituent quark mass can now be calculated, if we exchange the bare quark mass m with the constituent quark mass M .

$$S_M(p) = \frac{\not{p} + M}{p^2 - M^2 + i\epsilon}. \quad (1.16)$$

By applying the Dyson-equation for the interaction (figure 1.2), the interacting propagator can be written as

$$S_M(p) = S_m(p) + S_m(p)(\Sigma)S_M(p). \quad (1.17)$$

The self energy Σ can be calculated via [10]

$$\Sigma = \sum_j \Gamma_j 2ig \int \frac{d^4p}{(2\pi)^4} \text{Tr}(\Gamma_j S_M(p)). \quad (1.18)$$

Here Γ_j denotes the respective interaction channels. In the NJL-Lagrangian (1.8), the two channels

$$\Gamma_\sigma = \mathbb{1} \quad \Gamma_\pi = i\gamma_5 \vec{\tau} \quad (1.19)$$

can be identified. Since the trace over the Pauli-matrices $\vec{\tau}$ vanishes, $\text{Tr}(\Gamma_\pi)$ does not contribute to the self-energy. Evaluating the Γ_π -channel yields

$$\text{Tr} \left(\frac{\not{p} + M}{p^2 - M^2 + i\epsilon} \right) = \frac{4N_c N_f M}{p^2 - M^2 + i\epsilon}. \quad (1.20)$$

Here, the Trace was evaluated in the respective color, flavor and Dirac space. $N_c = 3$ and $N_f = 2$ are the respective number of colors and flavors. It was also used, that the Trace over the γ -Matrices vanishes. Using this and equation (1.18), equation (1.14) can be written as

$$M = m + \Sigma = m + 8N_f N_c g i \int \frac{d^4 p}{(2\pi)^4} \frac{M}{p^2 - M^2 + i\epsilon}. \quad (1.21)$$

This equation is called "Gap-equation", because of its similarity to the BCS-theory. The integral $I_1 = \int \frac{d^4 p}{(2\pi)^4} \frac{M}{p^2 - M^2 + i\epsilon}$ can be simplified using the residue theorem. Evaluating equation (1.21) yields [4], [11]

$$M = m + 8N_f N_c M g \int_0^\infty \frac{dp}{(2\pi)^2} \frac{p^2}{E(p)} \quad (1.22)$$

with the energy $E(p) = \sqrt{p^2 + M^2}$. As one might notice, the integral on the right side does not converge. Nambu and Jona-Lasinio ([9]) solved this problem by proclaiming a form factor $F(p, \Lambda)$, which is applied to the gap equation.

$$M = m + 8N_f N_c M g \int_0^\infty \frac{dp}{(2\pi)^2} \frac{p^2}{E(p)} F(p, \Lambda) \quad (1.23)$$

$F(p, \Lambda)$ and Λ have to be chosen according to the problem [9]. There are various methods to choose the form factor and each method has its advantages and disadvantages and has to be chosen to fit the regarding problem. In this work and in following evaluations, a simple three-momentum-cut-off will be used. This method leaves the analytical structure of the equation intact, although it violates Lorentz-invariance [2]. Applying the cut-off to the equation (1.23) yields

$$M = m + 8N_f N_c M g \int_0^\Lambda \frac{dp}{(2\pi)^2} \frac{p^2}{E(p)}, \quad (1.24)$$

where Λ can be fitted to the model.

Constituent Quark Mass at nonzero Temperatures

Up until now, only the case $T = 0$ and $\mu = 0$ has been considered. At nonzero temperatures and chemical potentials the constituent quark mass will change. To evaluate M , the Matsubara-formalism will be used. Its basic idea is to replace the time-component of the integral with an imaginary time. At imaginary time $t = i\tau$, the time-evolution operator e^{iHt} takes the same form as the Boltzmann-faktor $e^{-\beta T}$ and can be treated analogously. At finite time and periodic boundary conditions, the eigenvalues of the Hamiltonian are discrete and take the form $\omega_n = (2n + 1)\pi T$ with $n \in \mathbb{Z}$. At nonzero chemical potential, they are shifted by μ . ω_n are called the fermionic Matsubara-Frequencies [1]. Hence we can replace the time component of the integral in equation (1.21) with a discrete sum over the fermionic Matsubara frequencies [11]

$$i \int \frac{d^4 p}{(2\pi)^4} f(p_0, p) \rightarrow -T \sum_n \int \frac{d^3 p}{(2\pi)^3} f(i\omega_n + \mu, p). \quad (1.25)$$

Here, (p_0, \vec{p}) denotes the four-vector momentum. Replacing this in equation (1.21) yields

$$M = m - 8N_f N_c g \sum_n \int \frac{d^3 p}{(2\pi)^3} \frac{M}{(i\omega_n + \mu)^2 - E(p)^2 + i\epsilon}. \quad (1.26)$$

Here, again, $E(p) = \sqrt{p^2 + M^2}$. Evaluation of the sum yields [11]

$$M = m + 8N_c N_f g M \int \frac{d^3 p}{(2\pi)^3} \frac{1}{2E(p)} \left(1 - \frac{1}{1 + e^{(E(p)-\mu)/T}} - \frac{1}{1 + e^{(E(p)+\mu)/T}} \right). \quad (1.27)$$

In this equation, we can identify the quark and antiquark occupation numbers n_q and $n_{\bar{q}}$

$$n_q = \frac{1}{1 + e^{(E(p)-\mu)/T}} \quad n_{\bar{q}} = \frac{1}{1 + e^{(E(p)+\mu)/T}}. \quad (1.28)$$

Hence, the gap equation can be written as

$$M = m + 8N_c N_f g M \int \frac{d^3 p}{(2\pi)^3} \frac{1}{2E(p)} (1 - n_q - n_{\bar{q}}). \quad (1.29)$$

1.2.4 Mean-field Approximation

To calculate the thermodynamic potential, mean-field-approximation will be used. In this approximation, the respective quark fields are developed around their expectation values. Those can be calculated to

$$\langle \bar{\psi} \gamma_5 \vec{\tau} \psi \rangle = -i \int \frac{d^4 p}{(2\pi)^4} \text{Tr}(\gamma_5 \vec{\tau} S_M(p)) \quad (1.30)$$

and

$$\langle \bar{\psi} \psi \rangle = -i \int \frac{d^4 p}{(2\pi)^4} \text{Tr} S_M(p). \quad (1.31)$$

As was shown before, the first expression vanishes, since the trace of the Pauli-matrices vanish. The second equation defines the chiral condensate, a property, we will focus on later. It is connected with the constituent quark mass with equation (1.18) and (1.14). This yields

$$\langle \bar{\psi} \psi \rangle = -\frac{M - m}{2g}. \quad (1.32)$$

Mean-field-approximation is now applied by developing the interaction terms of the Lagrangian in first order [2]

$$\bar{\psi} \psi = \langle \bar{\psi} \psi \rangle + \delta_{\bar{\psi} \psi}. \quad (1.33)$$

Here $\delta_{\bar{\psi} \psi}$ denotes a small perturbation. Using this yields

$$(\bar{\psi} \psi)^2 = \langle \bar{\psi} \psi \rangle^2 + 2\langle \bar{\psi} \psi \rangle \delta_{\bar{\psi} \psi} + \delta_{\bar{\psi} \psi}^2 \approx -\langle \bar{\psi} \psi \rangle^2 + 2\langle \bar{\psi} \psi \rangle (\bar{\psi} \psi). \quad (1.34)$$

In the last step, all terms with order $\delta_{\bar{\psi}\psi}^2$ have been neglected. Now, the NJL-Lagrangian (1.8) in mean-field approximation can be specified to

$$\mathcal{L}_{MF} = \bar{\psi}(i\cancel{\partial} - m + 2g\langle\bar{\psi}\psi\rangle)\psi - g\langle\bar{\psi}\psi\rangle^2. \quad (1.35)$$

Using the constituent quark mass M in equation (1.32), the Lagrangian can be further written as

$$\mathcal{L}_{MF} = \bar{\psi}(i\cancel{\partial} - M)\psi - \frac{(M - m)^2}{4g}. \quad (1.36)$$

All further calculations will be made in mean-field approximation.

1.2.5 Thermodynamic Potential

With the Lagrangian in mean-field approximation, we can now proceed to determine the thermodynamic potential. The grand potential is given by [12]

$$\Omega(T, \mu, V) = -\frac{T}{V} \ln(\mathcal{Z}) = -\frac{T}{V} \ln \text{Tr} \left(\exp \left(-\frac{1}{T} \int d^4x (\mathcal{H} - \mu\mathcal{N}) \right) \right). \quad (1.37)$$

Here, \mathcal{H} denotes the Hamiltonian density, \mathcal{N} the particle density and \mathcal{Z} the grand canonical partition function. In mean-field approximation, the Hamiltonian density can be written as

$$\mathcal{H} = \bar{\psi}(-i\vec{\gamma}\vec{\nabla} + M)\psi + \frac{(M - m)^2}{4g} \quad (1.38)$$

The particle density can be written as

$$\mathcal{N} = \bar{\psi}\gamma_0\psi. \quad (1.39)$$

Using that, the grand potential can be written as

$$\Omega(T, \mu, V, M) = -\frac{T}{V} \ln \text{Tr} \exp \left(-\frac{1}{T} \int d^3x \left(\bar{\psi}(-i\vec{\gamma}\vec{\nabla} + M)\psi - \mu\bar{\psi}\gamma_0\psi + \frac{(M-m)^2}{4g} \right) \right). \quad (1.40)$$

This can now be separated in a free potential and an additional part, yielding

$$\Omega(T, \mu, V, M) = \Omega_{free}(T, \mu, V, M) + \frac{(M-m)^2}{4g} \quad (1.41)$$

with

$$\Omega_{free}(T, \mu, V, M) = -\frac{T}{V} \ln \text{Tr} \exp \left(-\frac{1}{T} \int d^3x \left(\bar{\psi}(-i\vec{\gamma}\vec{\nabla} + M)\psi - \mu\bar{\psi}\gamma_0\psi \right) \right). \quad (1.42)$$

As can be seen, $\Omega_{free}(T, \mu, V, M)$ denotes the grand potential of a free fermionic gas. This can be taken from the literature, i.e [12]. By that, the thermodynamic potential can be written as

$$\begin{aligned} \Omega_{free}(T, \mu, V, M) = & -2N_f N_c \int \frac{d^3p}{(2\pi)^3} \left(E(p) + T \ln \left(1 + e^{-(E(p)+\mu)/T} \right) \right. \\ & \left. + T \ln \left(1 + e^{-(E(p)-\mu)/T} \right) \right). \end{aligned} \quad (1.43)$$

Applying the above mentioned regularization by a three-momentum-cut-off yields for the potential

$$\begin{aligned} \Omega(T, \mu, V, M) = & -\frac{N_f N_c}{\pi^2} \left(\int_0^\Lambda dp p^2 E(p) + \int_0^\infty dp p^2 T \ln \left(1 + e^{-(E(p)-\mu)/T} \right) \right. \\ & \left. + T \ln \left(1 + e^{-(E(p)+\mu)/T} \right) \right) + \frac{(M-m)^2}{4g}. \end{aligned} \quad (1.44)$$

The cut-off was only applied to the vacuum part of the equation, since the remaining parts converge. As can be seen from the grand potential (1.37), it should follow [2]

$$\frac{d\Omega}{dm} = \frac{M-m}{2g} = \langle \bar{\psi}\psi \rangle. \quad (1.45)$$

Thus, interpreting $M = M(T, \mu, m)$ yields

$$\frac{d\Omega}{dm} = \frac{\partial\Omega}{\partial m} + \frac{\partial\Omega}{\partial M} \frac{\partial M}{\partial m} = \langle \bar{\psi}\psi \rangle + \frac{\partial\Omega}{\partial M} \frac{\partial M}{\partial m}. \quad (1.46)$$

Hence, consistency with equation (1.45) requires the gap equation

$$\frac{\partial\Omega}{\partial M} = 0. \quad (1.47)$$

This equation reproduces the gap equation (1.29). In a thermodynamic equilibrium, $\Omega(T, V, \mu, M)$ is therefore minimized over M . In general this equation has more than one solution. Of this solutions the minimal solution must be chosen. Solving this, the constituent quark mass can be determined for the respective T and μ .

1.2.6 Parameters

To complete the model, the necessary parameters must be found. Those are the cut-off Λ , the strong coupling constant g and the bare quark mass m . These parameters depend on each other and there are several possibilities to choose them. They can be determined with a fit by using the well known pion decay constant f_π and the pion mass m_π . In this work, the parameters used are arbitrarily taken from [2] and are depicted in the following table.

Parameters of the NJL model		
Λ in MeV	m in MeV	$g\Lambda^2$
587.9	5.6	2.44

1.2.7 Imaginary chemical potential

As it was mentioned before, in this work, the results shall be compared with lattice QCD results at imaginary chemical potential. For that, we have to calculate the thermodynamical potential at imaginary chemical potential as well. In order to do that, we replace μ with

$$\mu = i\Theta T. \quad (1.48)$$

Replacing μ in the thermodynamical potential (1.44) and using $\cos(\Theta) = \frac{1}{2}(e^{-i\Theta} + e^{i\Theta})$ yields

$$\Omega(M, T, \Theta) = \frac{(M - m)^2}{4g} - \frac{N_f N_c}{(\pi^2)} \left(\int_0^\Lambda dp p^2 E(p) + \int_0^\infty dp p^2 T \ln \left(1 + 2 \cos(\Theta) e^{-E(p)/T} + e^{-2E(p)/T} \right) \right) \quad (1.49)$$

As can be seen, the thermodynamic potential is always real. Further, it can be seen easily, that it is periodic with respect to Θ and follows the same symmetries as the cosine

$$\Omega(M, T, \Theta) = \Omega(M, T, \Theta + 2\pi) \quad (1.50)$$

and

$$\Omega(M, T, \Theta) = \Omega(M, T, -\Theta). \quad (1.51)$$

The corresponding gap equation is the same as for the real potential $\frac{\partial \Omega}{\partial M} = 0$ and can be found in appendix A.

1.2.8 Phase Transitions

As mentioned before, the chiral condensate is the order parameter for the chiral phase. A change in the chiral condensate is therefore a signal for a phase transition. In the NJL model, the constituent quark mass is closely related to the chiral condensate by equation (1.32) and can therefore taken as alternative order parameter. Solving the gap equation, it might be noticed, that a stable solution can turn unstable or vice versa. This can be seen in a discontinuity for M in the $T - \mu$ -plane. Such a discontinuity is a signal for a first order phase transition. Another possible change in the constituent quark mass is a smooth transition from a high constituent quark mass to almost zero (in the chiral limes, one would expect it to fall exactly to zero) [2]. This can be identified with a second order or crossover phase transition.

In the case of the chiral phase transition, we expect to find a first order transitions at lower temperatures and higher chemical potential and a smooth chiral crossover at higher temperatures [8]. In a critical point, the first order transition is expected to turn into the

crossover transition.

As a criterion for the transition, the chiral susceptibility can be chosen. The chiral susceptibility here will be defined as [3]

$$\chi_m = -\frac{\partial^2 \Omega}{\partial m^2} = -\frac{\partial}{\partial m} (\langle \bar{\psi} \psi \rangle). \quad (1.52)$$

In the NJL-model using equation (1.32), the chiral susceptibility can be calculated to

$$\chi_m = -\frac{1}{2g} \left(1 - \frac{\partial M}{\partial m} \right). \quad (1.53)$$

M can be taken from equation (1.29). χ is expected to be maximal at the phase transition line. Furthermore, the peak height and width can be considered as a measure for the broadness of the crossover transition. At the critical point, the susceptibility is expected to diverge [13]. The corresponding equation can be found in appendix A.

1.3 The PNJL Model

As mentioned above, the NJL model does not include a description of confinement. It is sufficient to describe the chiral phase transition, but there can no conclusions about confinement or deconfinement transitions be made. Therefore, an expanded model was proposed to address this problem. The PNJL model redefines the NJL Lagrangian by adding an effective gluon potential, which is expressed with the Polyakov-Loop. At imaginary chemical potential, the NJL model does not follow the periodicity of QCD. The PNJL model however is introduced, to fix this problem. It also contains the Z(3)-symmetry of QCD [14].

1.3.1 The Polyakov-Loop

The Polyakov Loop L is a matrix in color space and is an operator related to the gluon field. It is defined as [14]

$$L(\vec{x}) = \mathcal{P} \exp \left(i \int_0^\beta d\tau A_4(\vec{x}, \tau) \right), \quad (1.54)$$

where \mathcal{P} denotes the euclidean path ordering, $\beta = \frac{1}{T}$ and $A_4(\vec{x}, \tau)$ the fourth component of the gauge field. Choosing the Polyakov gauge, the matrix can be written in diagonal form as [15]

$$L = \exp(i\beta(\phi_3\lambda_3 + \phi_8\lambda_8)). \quad (1.55)$$

Here, ϕ_3 and ϕ_8 are real independent variables while λ_3 and λ_8 denote the respective Gell-Mann matrices. In the NJL-model, the Z(3) center symmetry, which denotes confinement, is not included. However, the Z(3) symmetry is an important symmetry, which is broken at high temperatures [16]. The Polyakov loop can now be used to define the order parameter of said symmetry. For that, it is convenient to define the following quantities

$$\Phi = \frac{1}{N_c} \text{Tr}_c L \quad \text{and} \quad \bar{\Phi} = \frac{1}{N_c} \text{Tr}_c L^\dagger. \quad (1.56)$$

The expectation values of Φ and $\bar{\Phi}$ can also be written as [14]

$$\Phi = \exp\left(-\frac{F_q}{T}\right) \quad \bar{\Phi} = \exp\left(-\frac{F_q^*}{T}\right), \quad (1.57)$$

where F_q and F_q^* is the free energy of a static quark and antiquark [16]. In the confined phase, $F_q = F_q^* = \infty$, therefore it is not possible to create a single quark, hence $\Phi = \bar{\Phi} = 0$. It is however possible in the deconfined phase, where the free energy is finite and Φ and $\bar{\Phi}$ are non-zero and the Z(3) symmetry is spontaneously broken [16]. This denotes the nature of the Z(3) symmetry. Therefore, $\Phi = \bar{\Phi} = 0$ can be identified with the confined phase. This is the case at low temperatures and low chemical potentials. If $\Phi \neq 0$ and $\bar{\Phi} \neq 0$, then this can be identified as the deconfined phase [14].

1.3.2 Lagrangian of the PNJL model

Taken this into account, we can now move on to define the Lagrangian of the PNJL model by using the expectation values of the Polyakov loop as order parameter. In the PNJL-model, the Lagrangian is defined as [17]

$$\mathcal{L}_{PNJL} = \bar{\psi}(i\not{D} - \hat{m})\psi + g[(\bar{\psi}\psi)^2 + (\bar{\psi}i\gamma_5\vec{\tau}\psi)^2] + \mathcal{U}(\Phi, \bar{\Phi}, T). \quad (1.58)$$

This is analogue to the NJL-Lagrangian (1.8). Here, the covariant derivative can be expressed as

$$D_\mu = \partial_\mu - i\delta_\mu^0 A_0^a t^a. \quad (1.59)$$

$\mathcal{U}(\Phi, \bar{\Phi}, T)$ is an effective gluon potential. There are various ansätze for $\mathcal{U}(\Phi, \bar{\Phi}, T)$. In this work, we will use the ansatz from [17]

$$\mathcal{U}(\Phi, \bar{\Phi}, T) = -\frac{1}{2}T^4 a(T)\bar{\Phi}\Phi + T^4 b(T) \ln\left(1 - 6\Phi\bar{\Phi} + 4(\Phi^3 + \bar{\Phi}^3) - 3(\bar{\Phi}\Phi)^2\right) \quad (1.60)$$

with

$$a(T) = a_0 + a_1 \left(\frac{T_0}{T}\right) + a_2 \left(\frac{T_0}{T}\right)^2 \quad \text{and} \quad b(T) = b_3 \left(\frac{T_0}{T}\right)^3. \quad (1.61)$$

$\mathcal{U}(\Phi, \bar{\Phi}, T)$ is constructed to satisfy the Z(3) symmetry.

In the literature, i.e [17], T_0 is often chosen to be 270 MeV. This enforces a phase transition of a gluon plasma without quarks at 270 MeV. However, considering quarks, T_0 becomes smaller [18]. In [19], T_0 for two flavors in the limes of massless quarks was calculated to be $T_0 = 208$ MeV. However, this value has a great uncertainty. In this work, the respective parameters are taken from [4] and can be seen in the following table.

Parameters of $\mathcal{U}(\bar{\Phi}, \Phi, T)$				
a_0	a_1	a_2	b_3	T_0
3.51	-2.47	15.2	-1.75	212 MeV

On a notice, because of the chosen ansatz it must hold that $\Phi < 1$ and $\bar{\Phi} < 1$ since otherwise the logarithm turns negative or diverges. The parameters were obtained by fitting results to the results of pure gauge theory and the Polyakov loop [17].

1.3.3 The Thermodynamic Potential

Obtaining the thermodynamic potential in the PNJL model is similar to the NJL model. First, we will express the Lagrangian in mean-field approximation. Doing so, we obtain

$$\mathcal{L}_{PNJL} = \bar{\psi}(i\mathcal{D} + M)\psi - 2g\sigma^2 + \mathcal{U}(\Phi, \bar{\Phi}, T) \quad (1.62)$$

Here, we defined $\sigma = \langle \bar{\psi}\psi \rangle$. For determining the thermodynamic potential, we have to consider the Polyakov loop. The Trace in color space has now to be evaluated separately. This leads to [14]

$$\begin{aligned} \Omega_{PNJL}(\sigma, \Phi, \bar{\Phi}, T, \mu) = & \mathcal{U}(\Phi, \bar{\Phi}, T) + g\sigma^2 - 2N_f N_c \int \frac{d^3p}{(2\pi)^3} E(p) \\ & - 2N_f T \int \frac{d^3p}{(2\pi)^3} \left(\text{Tr}_c \ln \left(1 + L e^{-(E(p)+\mu)/T} \right) \right. \\ & \left. + \text{Tr}_c \ln \left(1 + L^\dagger e^{-(E-\mu)/T} \right) \right). \end{aligned} \quad (1.63)$$

Evaluating the remaining traces in color space yields

$$\begin{aligned} \Omega_{PNJL}(\sigma, \Phi, \bar{\Phi}, T, \mu) = & \mathcal{U}(\Phi, \bar{\Phi}, T) + g\sigma^2 - \frac{N_f N_c}{\pi^2} \int_0^\Lambda dp p^2 E(p) \\ & - \frac{N_f}{\pi^2} \int_0^\infty dp p^2 T \\ & \left(\ln \left(1 + 3\Phi e^{-(E(p)-\mu)/T} + 3\bar{\Phi} e^{-2(E(p)-\mu)/T} + e^{-3(E(p)-\mu)/T} \right) \right. \\ & \left. + \ln \left(1 + 3\bar{\Phi} e^{-(E(p)+\mu)/T} + 3\Phi e^{-2(E(p)+\mu)/T} + e^{-3(E(p)+\mu)/T} \right) \right). \end{aligned} \quad (1.64)$$

Again, the cut-off was applied. A more detailed calculation is presented in appendix B. Here as well applies the relation $\frac{d\Omega}{dm} = \sigma$. So in this case, the gap equations are

$$\frac{\partial \Omega_{PNJL}}{\partial \sigma} = 0 \quad \frac{\partial \Omega_{PNJL}}{\partial \Phi} = 0 \quad \frac{\partial \Omega_{PNJL}}{\partial \bar{\Phi}} = 0. \quad (1.65)$$

The exact expressions can be found in appendix B. Here, the thermodynamic potential Ω is minimized with respect to the order parameters σ , Φ and $\bar{\Phi}$. The minimal solution will be interpreted as the stable solution. In analogy to the NJL-model the parameters Λ , g and m for the PNJL model have to be determined. Those can be taken from [4] and are depicted in the following table.

Parameters of the PNJL model		
Λ in MeV	m in MeV	$g\Lambda^2$
631.5	5.5	2.1925

Again, these parameters were fitted to reproduce the pion decay constant $f_\pi = 92.4$ MeV and the pion mass $m_\pi = 135.0$ MeV.

1.3.4 Imaginary chemical potential

To move on to imaginary chemical potential, we again will use equation (1.48) to replace the chemical potential in the grand potential. Here, it is convenient to additionally replace Φ and $\bar{\Phi}$ with [4]

$$\Phi = \Psi e^{i\Theta} \quad \bar{\Phi} = \bar{\Psi} e^{-i\Theta}. \quad (1.66)$$

Applying those to the PNJL thermodynamic potential (1.64) yields

$$\begin{aligned} \Omega_{PNJL}(\sigma, \Psi, \bar{\Psi}, T, \Theta) = & \mathcal{U}(\Psi, \bar{\Psi}, T) + g\sigma^2 - \frac{N_f N_c}{\pi^2} \int_0^\Lambda dp p^2 E(p) \\ & - \frac{N_f}{\pi^2} \int_0^\infty dp p^2 T \\ & \left(\ln \left(1 + 3\Psi e^{-E(p)/T} + \left(3\bar{\Psi} e^{-2E(p)/T} + e^{-3E(p)/T} \right) e^{3i\Theta} \right) \right. \\ & \left. + \ln \left(1 + 3\bar{\Psi} e^{-E(p)/T} + \left(3\Psi e^{-2E(p)/T} + e^{-3E(p)/T} \right) e^{-3i\Theta} \right) \right) \end{aligned} \quad (1.67)$$

with

$$\mathcal{U}(\Psi, \bar{\Psi}, T) = -\frac{a(T)}{2}T^4\Psi\bar{\Psi} + b(T)T^4 \ln\left(1 - 6\Psi\bar{\Psi} + 4(\Psi^3 e^{-3i\Theta} + \bar{\Psi}^3 e^{3i\Theta}) - 3(\Psi\bar{\Psi})^2\right). \quad (1.68)$$

As can be seen, Θ only contributes in form of $e^{-3i\Theta}$ and $e^{3i\Theta}$. Hence, the thermodynamic potential is symmetric in the form

$$\Omega_{PNJL}(\sigma, \Psi, \bar{\Psi}, T, \Theta) = \Omega_{PNJL}(\sigma, \Psi, \bar{\Psi}, T, \Theta + \frac{2\pi}{3}). \quad (1.69)$$

This periodicity is also known as the Roberge Weiss periodicity [4]. It also holds, that for minimal solutions Ψ and $\bar{\Psi}$ must follow the same transition. Furthermore, the thermodynamic potential has to be real. To ensure that, it must hold, that

$$\Psi = \bar{\Psi}^* \quad (1.70)$$

Then, we can write the quantities Φ and $\bar{\Phi}$ as

$$\Phi = |\Psi|e^{i\phi} \quad \text{and} \quad \bar{\Phi} = |\Psi|e^{-i\phi} \quad (1.71)$$

with a phase angle ϕ . Putting all of this together, we obtain the thermodynamic potential

$$\begin{aligned} \Omega_{PNJL}(\sigma, \Psi, \bar{\Psi}, T, \Theta) = & g\sigma^2 + \mathcal{U}(|\Psi|, \phi, \Theta) \\ & - \frac{N_f N_c}{\pi^2} \int_0^\Lambda dp p^2 E(p) \\ & - \frac{N_f}{\pi^2} \int_0^\infty dp p^2 T \ln \left(1 + e^{-6E(p)/T} + 6|\Psi| \cos \phi \left(e^{-E(p)/T} + e^{-5E(p)/T} \right) \right. \\ & + (9|\Psi|^2 + 6|\Psi| \cos(\phi - 3\Theta)) \left(e^{-2E(p)/T} + e^{-4E(p)/T} \right) \\ & \left. + (18|\Psi|^2 \cos(3\Theta - 3\phi) + 2 \cos(3\Theta)) e^{-3E(p)/T} \right) \end{aligned} \quad (1.72)$$

with

$$\mathcal{U}(|\Psi|, \phi, \Theta) = -\frac{a(T)}{2}T^4|\Psi|^2 + b(T)\ln(1 - 6|\Psi|^2 + 8|\Psi|^3 \cos(3\phi - 3\Theta) - 3|\Psi|^4). \quad (1.73)$$

Thus, leading to the gap equations

$$\frac{\partial\Omega_{PNJL}}{\partial\sigma} = 0 \quad \frac{\partial\Omega_{PNJL}}{\partial\phi} = 0 \quad \frac{\partial\Omega_{PNJL}}{\partial|\Psi|} = 0. \quad (1.74)$$

The exact expression can again be found in appendix B. As for the real chemical potential, those have to be solved and the solution, which minimizes the thermodynamic potential, has to be chosen.

1.3.5 Phase transitions

The susceptibilities for the PNJL-model can be calculated in a similar manner. Now, the chiral condensate is given by $\sigma = \sigma(\Phi, \bar{\Phi})$. Hence, the chiral susceptibility χ_m is more difficult to calculate. Therefore, in this work, the susceptibilities will be calculated numerically.

Regarding the symmetry of the thermodynamic potential (1.72), it must hold

$$\Omega_{PNJL}(\sigma, \Psi, \bar{\Psi}, T, \Theta) = \Omega_{PNJL}(\sigma, \Psi, \bar{\Psi}, T, -\Theta) \quad (1.75)$$

as well as the before mentioned relation

$$\Omega_{PNJL}(\sigma, \Psi, \bar{\Psi}, T, \Theta) = \Omega_{PNJL}(\sigma, \Psi, \bar{\Psi}, T, \Theta + \frac{2\pi}{3}). \quad (1.76)$$

So the thermodynamic potential is a periodic function with a period of $\frac{2\pi}{3}$ with respect to Θ . However, the value Ψ has the properties [15]

$$\Psi(\Theta) = \Psi\left(\Theta + \frac{2\pi}{3}\right) \quad \text{and} \quad \Psi(\Theta)^* = \Psi\left(\Theta + \frac{2\pi}{3}\right)^*. \quad (1.77)$$

Furthermore, by the construction we did in equation (1.71) and considering the real part and imaginary part of Ψ yield the symmetries

$$\begin{aligned}\operatorname{Im} \Psi(\Theta) &= \frac{\Psi(\Theta) - \Psi(\Theta)^*}{2i} = -\operatorname{Im} \Psi(-\Theta) \\ \operatorname{Re} \Psi(\Theta) &= \frac{\Psi(\Theta) + \Psi(\Theta)^*}{2} = \operatorname{Re} \Psi(\Theta).\end{aligned}\tag{1.78}$$

Hence, the imaginary part of Ψ is an odd function, whilst the real part is an even function [15]. In the vicinity of $\Theta = \frac{\pi}{3}$, by the previous considerations, it therefore must yield

$$\operatorname{Im} \Psi\left(\frac{\pi}{3} - \epsilon\right) = -\operatorname{Im} \Psi\left(\frac{\pi}{3} + \epsilon\right).\tag{1.79}$$

Hence, if $\operatorname{Im} \Psi\left(\frac{\pi}{3}\right) \neq 0$, there must be a discontinuity at $\Theta = \frac{\pi}{3}$, thus leading to a first order phase transition. This transition, known as the Roberge Weiss transition, is, as well as the Roberge Weiss periodicity, also present in lattice QCD [15].

2 Phase Transitions in the NJL model

2.1 Solving the gap equation at real chemical potential

Here, the gap equation for the NJL model 1.47 were solved. The constituent quark mass M was determined in the μ - T plain for a finite bare quark mass and the chiral limes ($m = 0$). The solutions can be seen in figure 2.1.

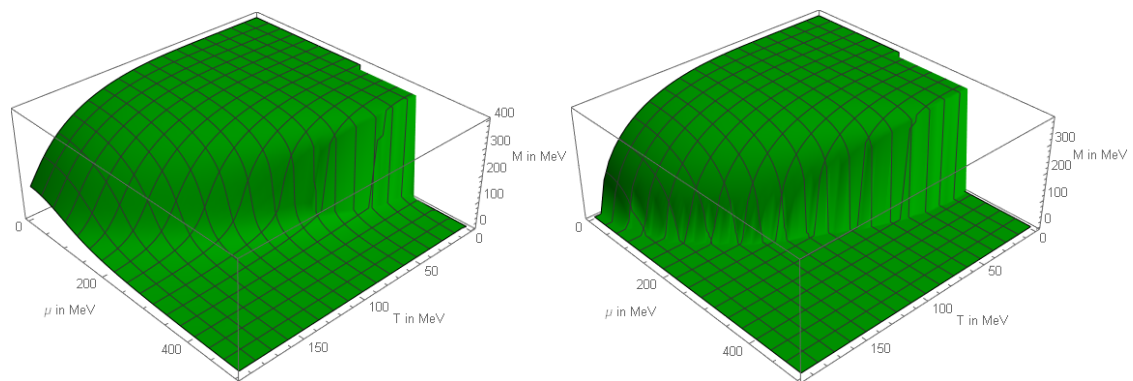


Figure 2.1: The constituent quark mass in the NJL model as a function of T and μ . On the left, the quark mass was finite, on the right, the bare quark mass was taken to zero.

For low temperatures and finite bare quark mass, there is a sharp and discontinuous decline in the constituent quark mass. This will be interpreted as a first order chiral phase transition. M is high in vacuum, when chiral symmetry is spontaneously broken and close to zero, when chiral symmetry is restored. For higher temperatures, the decline becomes smoother and turns eventually into a crossover transition. There is a critical point, where the transition turns from a first order phase transition to a smooth crossover.

In the chiral limes, the transition is more rapid. The phase transition is also first order

for low temperatures. For higher temperatures, the transition becomes a second order transition. All future calculations are conducted for non-vanishing quark masses.

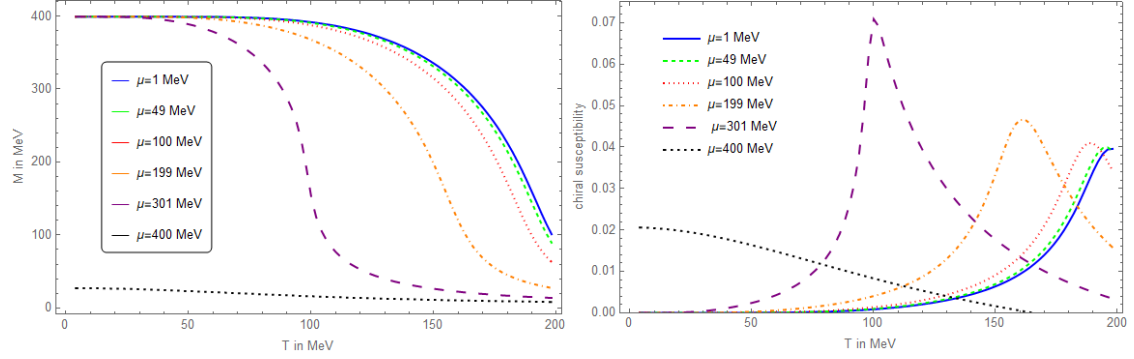


Figure 2.2: At the left, the constituent quark mass is presented as a function of the Temperature at fixed chemical potential. On the right, the chiral susceptibility is presented as a function of the temperature at fixed chemical potential.

In figure 2.2 the solutions for various fixed chemical potential can be seen. For higher chemical potentials the phase transition turns wider until it vanishes completely. This can also be seen at the broadness of the peak in the chiral susceptibility. For a better comparison later with Lattice QCD results, the susceptibility χ_m and the chiral condensate will be renormalized in the following way

$$\begin{aligned}\chi_{m,re} &= (\chi_m(T, \mu) - \chi_m(T = 0, \mu = 0)) \frac{m^2}{f_\pi^4} \\ \sigma_{re} &= (\sigma(T, \mu) - \sigma(T = 0, \mu = 0)) \frac{m}{f_\pi^4}.\end{aligned}\tag{2.1}$$

We followed the same renormalization as in [3].

In figure 2.3 the solutions for fixed temperatures can be seen. At lower temperatures there is a first order phase transition, which can be seen clearly at the steep and discontinuous fall of the constituent quark mass. For higher temperatures, the transition turns into a much broader crossover transition. The chiral susceptibility for lower temperatures shows a discontinuity at the first order phase transition.

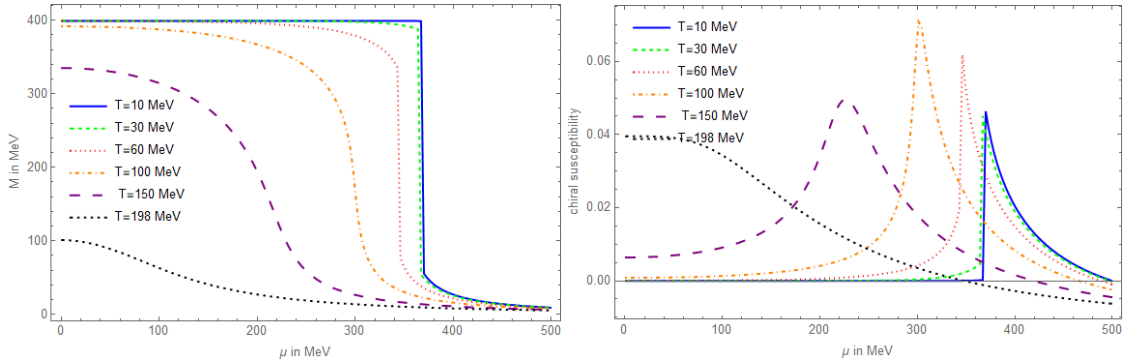


Figure 2.3: At the left, the constituent quark mass is presented as a function of the chemical potential for fixed temperatures. At the right, the chiral susceptibility is presented as a function of the chemical potential for various fixed temperatures.

2.1.1 The NJL phase diagram at real chemical potential

The criterion chosen for a phase transition was a maximum in the chiral susceptibility at constant T for lower chemical potentials and at constant μ for higher chemical potentials. We followed the same renormalization as in [3].

Now, we can determine the phase transition line. The results can be seen in figure 2.4. The critical point was determined by finding the temperature, at which there is no discontinuity in the chiral susceptibility or the constituent quark mass. It could be identified as $(T_c, \mu_c) = (81.3 \text{ MeV}, 322.8 \text{ MeV})$. This is the point, where the discontinuity of the constituent quark mass vanishes and the chiral susceptibility is maximal.

2.2 Solving the gap equation at imaginary chemical potential

Using equation 1.49, the gap equation for imaginary potential can now be solved.

The Solutions can be seen in figure 2.5. Here, there is no first order phase transition in the considered temperature range. The transition between the two phases is always a smooth crossover. Also, the symmetry around $\Theta = \pi$ can be seen.

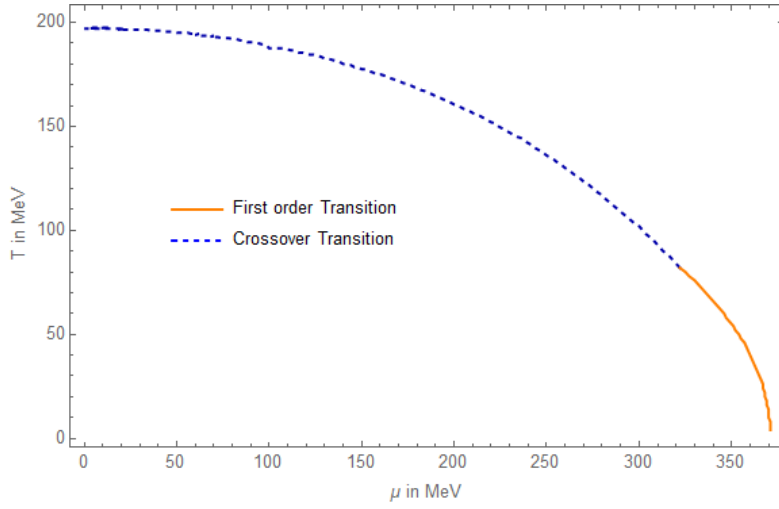


Figure 2.4: The phase diagram in the NJL model. The upper area represents the phase of restored chiral symmetry, the lower area of spontaneously broken chiral symmetry. At low temperatures, there is a first order phase transition. At higher temperatures, this turns into a crossover transition.

In figure 2.6, the constituent quark mass and the chiral susceptibility at constant temperatures can be seen. Again, the susceptibility peaks at the phase transition line. Also, the peak of the susceptibility becomes higher for higher temperatures, as the constituent quark mass decreases more sharply, but it still denotes a crossover transition. At lower temperatures, the constituent quark mass forms a plateau. At higher temperatures however the constituent quark mass either falls to nearly zero for small Θ or begins to grow for Θ near to $\Theta = \pi$.

In figure 2.7, the constituent quark mass and the chiral susceptibility at fixed Θ can be seen. At lower temperatures, we can observe a peak, denoting the phase transition. The peak is shifted to higher temperatures as Θ grows, until it eventually vanishes in the considered temperature range.

2.2.1 The NJL Phase diagram at imaginary chemical potential

Again, we chose the chiral susceptibility as a crossover criterion. The results can be seen in figure 2.8. Again, the symmetry around $\Theta = \pi$ is clearly visible. With those results,

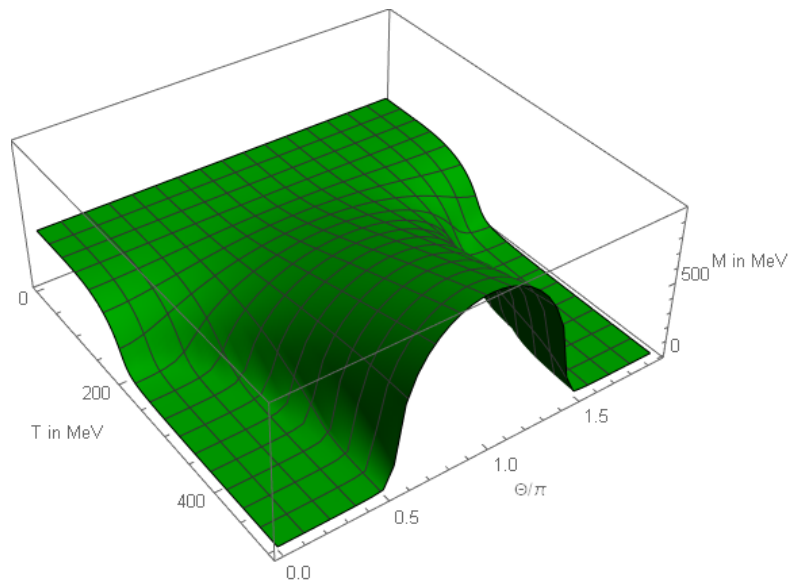


Figure 2.5: The solutions for the gap equation at imaginary chemical potential

we can now combine the solutions for real chemical potential and imaginary chemical potential and determine the phase transition line in the $\mu^2 - T$ plain. This can be seen in figure 2.9.

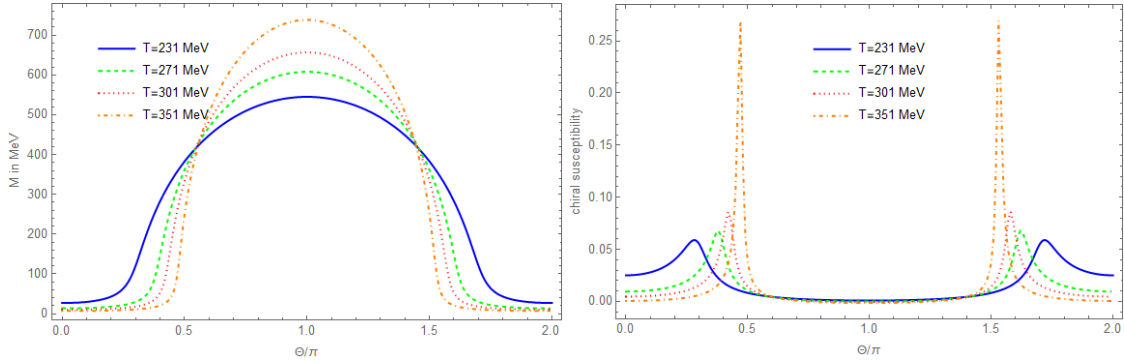


Figure 2.6: The constituent quark mass in the NJL model at imaginary chemical potential is presented as a function of Θ on the left, while the chiral susceptibility is presented as a function of Θ on the right. Both were done for various fixed temperatures.

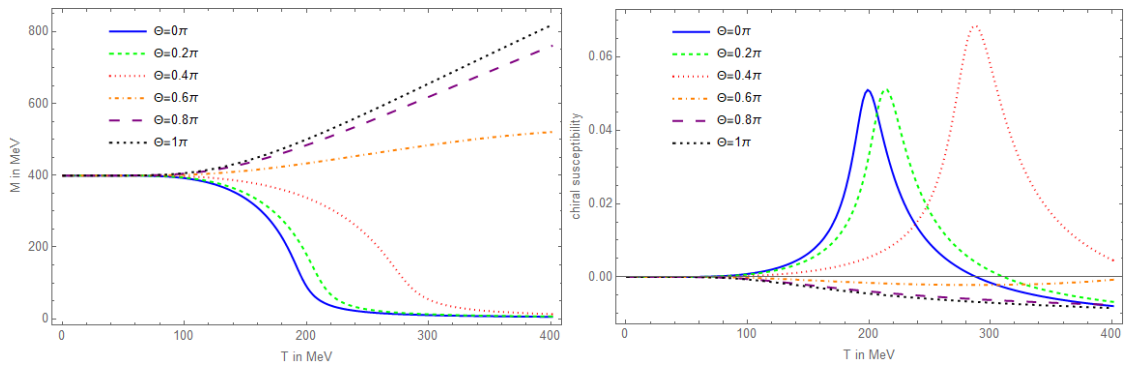


Figure 2.7: The constituent quark mass in the NJL model at imaginary chemical potential is presented as a function of T on the left, while the chiral susceptibility is presented as a function of T on the right. Both were done for various fixed Θ .

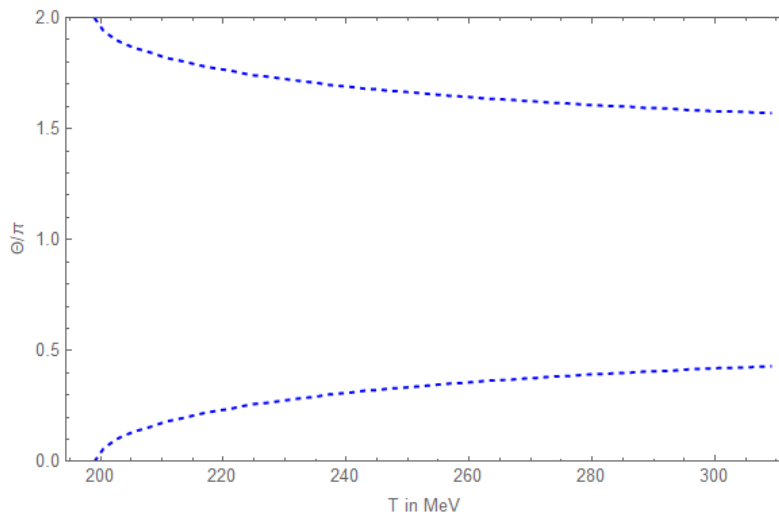


Figure 2.8: The phase transition lines in the NJL model at imaginary chemical potential in the $\Theta - T$ -plain.

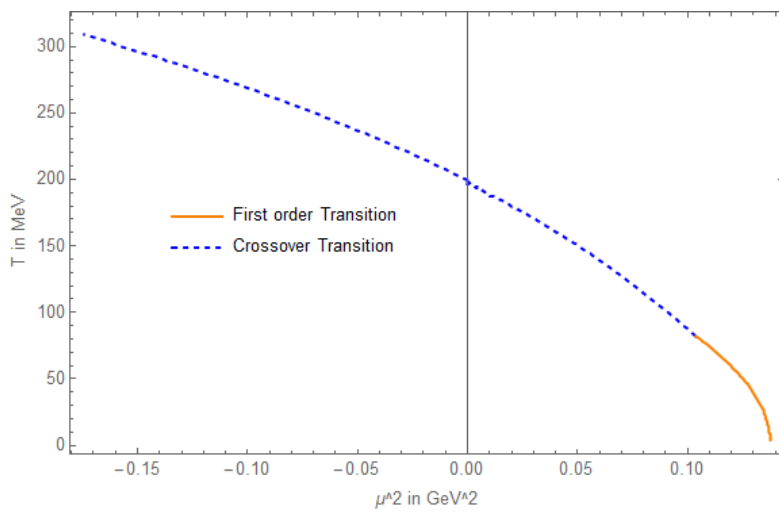


Figure 2.9: The phase transition lines in the NJL model in the $\mu^2 - T$ -plain. At imaginary chemical potential ($\mu^2 < 1$) there is just a crossover transition, while at real chemical potential there is also a first order phase transition at low temperatures.

3 Phase Transitions in the PNJL model

3.1 Solving the gap equation at real chemical potential

The solutions for the PNJL gap equations (1.65) can be seen in figure 3.1. The solutions for the chiral condensate are similar to the NJL model. There is also a first order phase transition at low temperatures and high chemical potentials, which turns into a smooth crossover at higher temperatures. The maximal chiral susceptibility at constant μ will, again, be the crossover transition criterion.

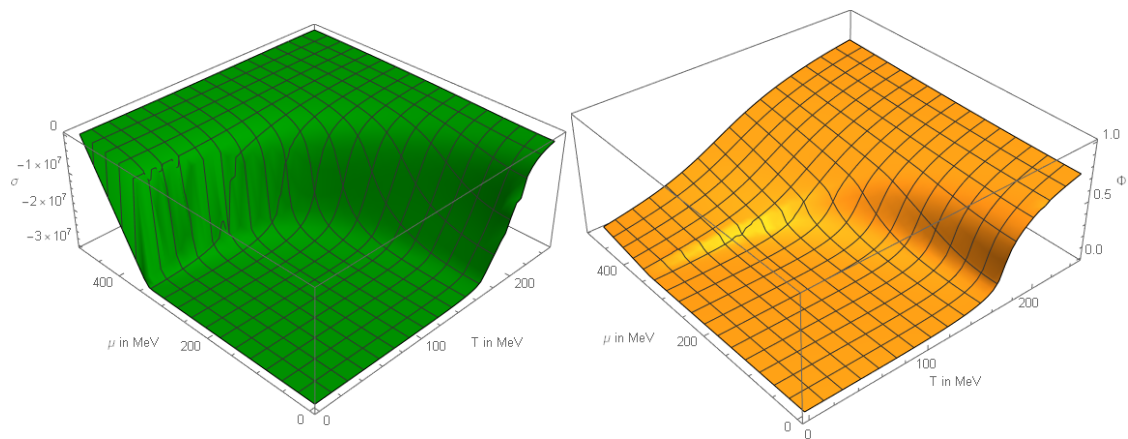


Figure 3.1: The chiral condensate σ (left) and the Polyakov loop expectation value Φ (right) in the $T - \mu$ -plain.

The Polyakov-loop Φ and $\bar{\Phi}$ serve as order parameter for the confined/deconfined phases. At low temperatures, those values are zero and can therefore be identified with the confined phase. If those values are nonzero, we are in the deconfined phase. At higher

temperatures, there is a crossover transitions from low to higher Φ . As transition criterion in this work, the point of the highest increase at constant chemical potential will be chosen.

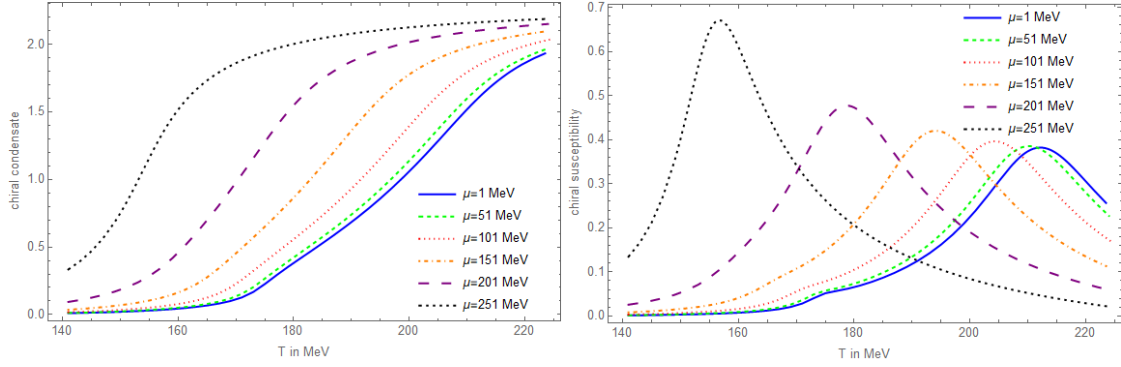


Figure 3.2: The renormalized chiral condensate (left) and the renormalized chiral susceptibilities (right) as functions of the temperature for various fixed chemical potentials.

In figure 3.2 the chiral condensate and the chiral susceptibility for fixed chemical potentials are presented. The chiral condensate and the chiral susceptibility have been renormalized as in equation (2.1). At low chemical potentials, there is a smooth crossover transition from low chiral condensate to high chiral condensate. The chiral susceptibility has a clearly visible peak at the point of highest increase. The peak gets higher at higher chemical potentials.

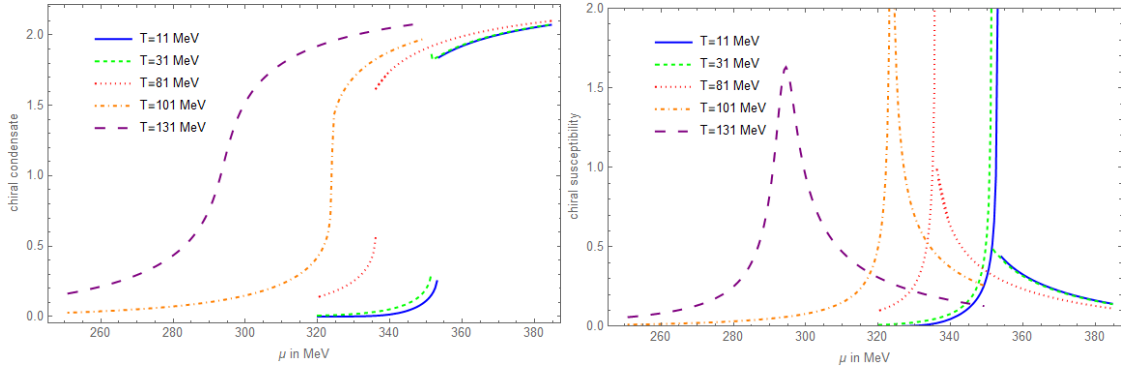


Figure 3.3: The renormalized chiral condensate (left) and the renormalized chiral susceptibilities as functions of μ for various fixed temperatures.

The chiral condensate and susceptibility for fixed temperatures are presented in figure 3.3. The first order phase transition becomes quite clear, because of the discontinuity of the chiral condensate and the chiral susceptibility. At higher temperatures, we can observe a crossover. The discontinuity vanishes and there is a divergence of the chiral susceptibility at the critical point. The critical point could be identified to be around $(T;\mu)=(103.5\text{ MeV};322\text{ MeV})$.

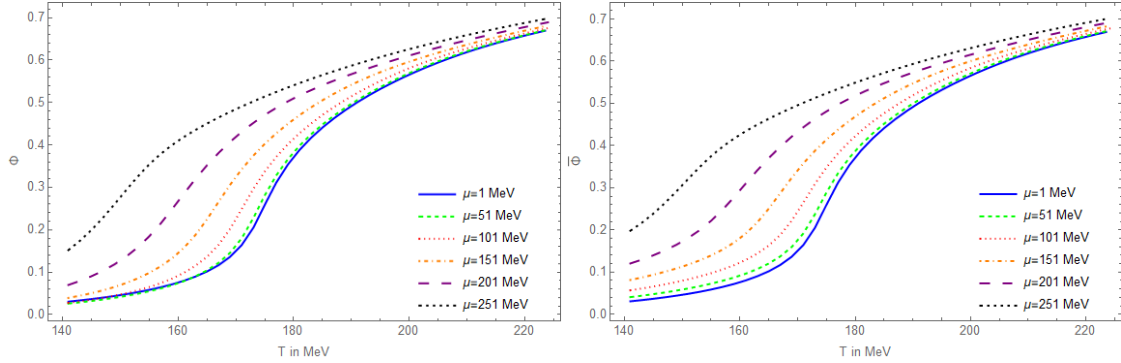


Figure 3.4: The Polyakov loop expectation values Φ and $\bar{\Phi}$ as a function of the temperature for various fixed chemical potentials.

The solutions for the Φ and $\bar{\Phi}$ are presented in figure 3.4. It can be seen, that the solutions for Φ and $\bar{\Phi}$ are nearly identical, so we will focus of Φ for future considerations. The value of Φ increases smoothly and can be denoted with a crossover transition.

For small temperatures and high chemical potentials (not depicted in the figure), the increase becomes relatively small, however, there is still a jump of Φ and $\bar{\Phi}$. This coincides directly with the first order chiral phase transition.

3.1.1 The PNJL phase diagram at real chemical potential

In the phase diagram, we will distinguish two separate phase transitions: The chiral and the deconfinement transition. The phase diagram can be seen in figure 3.5. At low chemical potentials, the confinement phase transition occurs at lower temperatures. The confinement phase transition joins with the chiral phase transition in the vicinity of the critical point. After that, they coincide. Furthermore, at lower chemical potentials, the increase of Φ becomes smaller. However, it can still be identified with a phase transition.

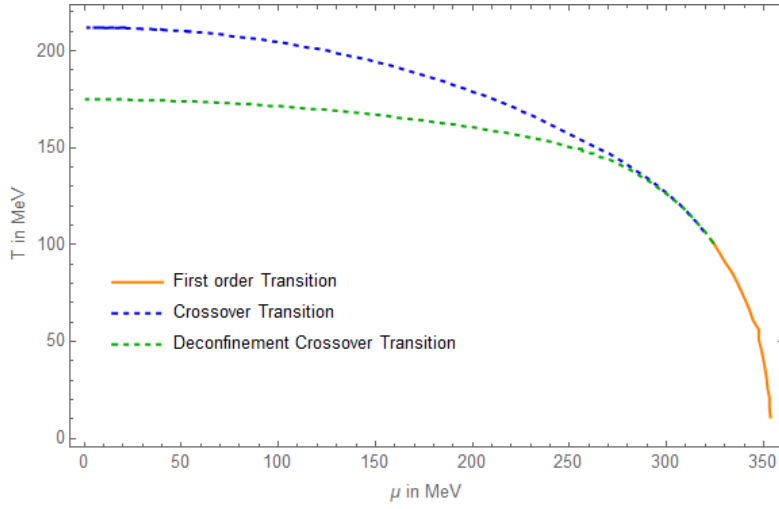


Figure 3.5: The phase transition lines for real chemical potential in the PNJL model. At lower temperatures there is a first order phase transition from the confined to the deconfined phase the phase of restored chiral symmetry. At higher temperatures there is a crossover for both phase transitions, while the deconfinement crossover occurs at lower temperatures.

3.2 Solving the gap equation at imaginary chemical potential

The gap equations at imaginary potential were also solved. Those results are fairly different from the results at imaginary chemical potentials in the NJL model. The Roberge Weiss periodicity can be observed. Furthermore, at $\Theta = \frac{\pi}{3}$, all order parameters show a discontinuity. This shows the Roberge Weiss phase transition mentioned before.

The Solutions for fixed Temperature can be seen in figure 3.6. The Roberge Weiss phase transition can be seen for higher temperatures as a cusp in the chiral condensate and $|\Psi|$ at $\Theta = \frac{\pi}{3}$. Also the phase angle ϕ at the transition line shows a discontinuity in the form of a jump from positive to negative values. However, this just occurs at higher temperatures. This Roberge Weiss phase transition begins to occur at a temperature of around $T = 189$ MeV.

The solutions for fixed Θ are presented in figure 3.7. The chiral condensate shows a smooth crossover transition for all Θ . For higher Θ , the transition is moved to higher temperatures. At the Roberge Weiss transition line, no chiral transition can be observed

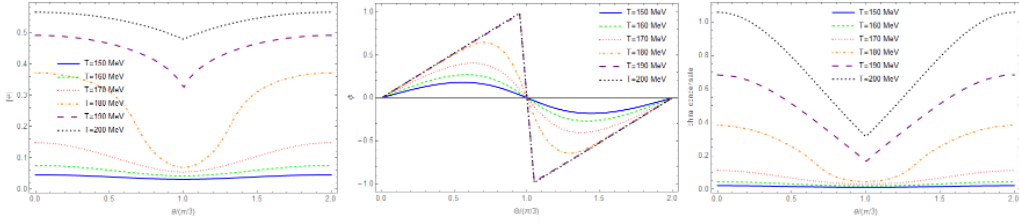


Figure 3.6: The solutions for $|\Psi|$, ϕ and the chiral condensate as a function of Θ for fixed temperatures in the PNJL model at imaginary chemical potential. There is a discontinuity at the first order Roberge Weiss phase transition at $\Theta = \frac{\pi}{3}$.

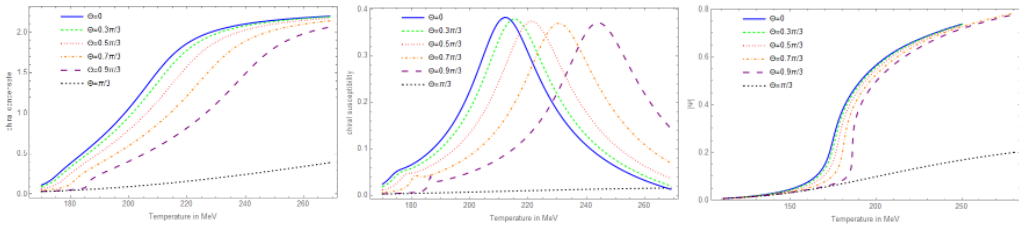


Figure 3.7: The chiral susceptibility, the chiral condensate and $|\Psi|$ as a function of the temperature for various fixed Θ in the PNJL model at imaginary chemical potential.

and the chiral condensate stays low for the considered temperature range. The chiral susceptibility shows a peak at the phase transition. This peak is for all Θ at approximately the same height and all curves show a similar broadness. As expected, the peak is shifted towards higher temperatures the closer Θ moves to the Roberge Weiss transition line. The deconfinement phase transition, represented by an increase of $|\Psi|$ is also a smooth crossover transition for all Θ . It also is shifted towards higher temperatures the closer Θ moves to the Roberge Weiss phase transition line.

3.2.1 The PNJL phase diagram at imaginary chemical potential

The phase diagram at imaginary chemical potential in the PNJL model can be seen in figure 3.8. The Roberge Weiss periodicity can also be seen. The deconfinement phase transition occurs at lower temperatures than the chiral phase transition. The closer Θ gets to $\frac{\pi}{3}$, the higher get the transition temperatures.

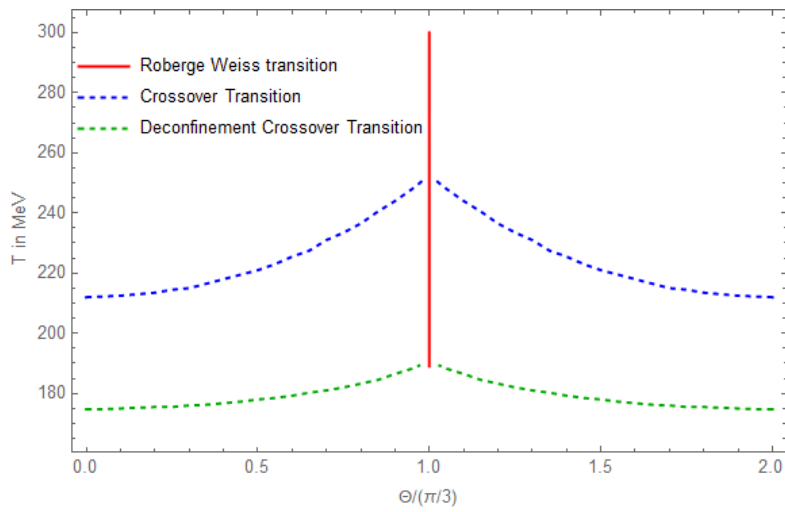


Figure 3.8: The phase diagram at imaginary chemical potential in the PNJL model in the $\mu - T$ -plane. The Roberge Weiss phase transition can be seen at $\Theta = \frac{\pi}{3}$ as the red line. The deconfinement crossover transition is represented by the green dashed line, while the chiral phase transition is represented by the blue dashed line.

Now, the complete phase diagram can be constructed. The diagram in the $\mu^2 - T$ -plane can be seen in figure 3.9.

It can be noted, that the transition from imaginary potential to real potential is smooth, so an extrapolation from imaginary to real chemical potential seems possible.

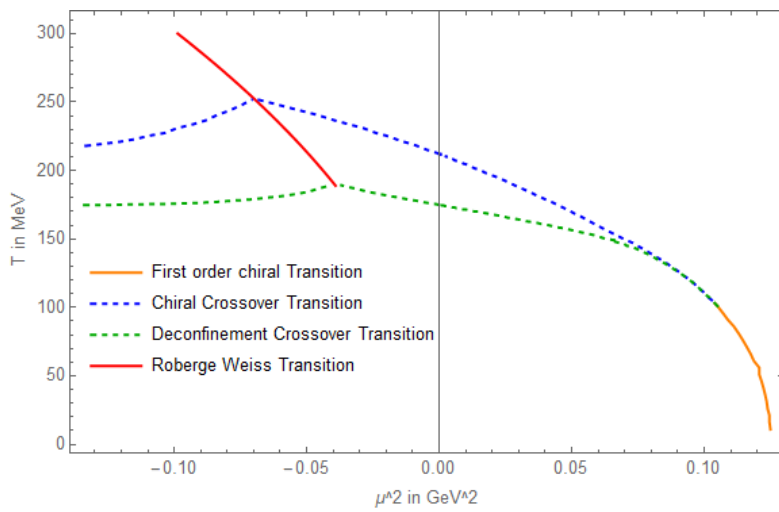


Figure 3.9: The complete phase diagram in the PNJL model in the $\mu^2 - T$ -plain. The red line denotes the Roberge Weiss phase transition, the green dashed line the deconfinement crossover transition, the blue dashed line the chiral crossover transition and the orange line the first order chiral phase transition.

4 Comparisons with Lattice QCD

Now the results of the previous sections can be compared with lattice QCD results. As mentioned, all results will be taken from [3]. In that work by Borsanyi et al., calculations were also conducted for two quark flavors in the isospin limes at imaginary chemical potential.

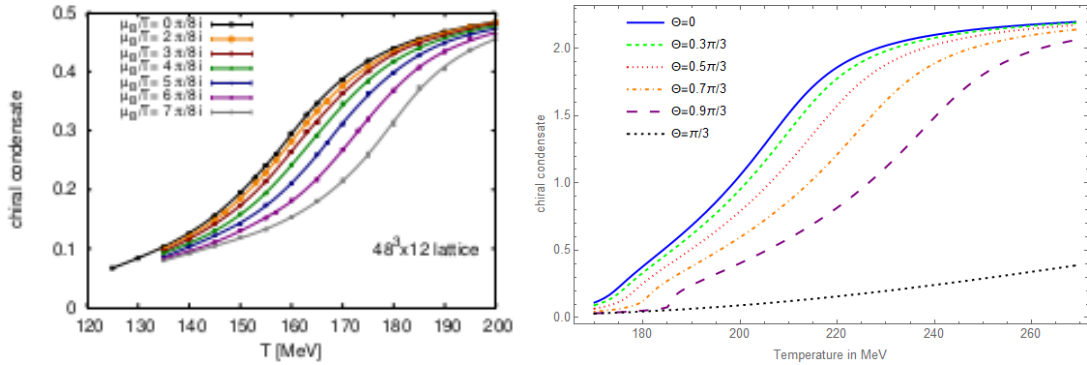


Figure 4.1: Comparison between QCD lattice results (left, taken from [3]) and calculations in the PNJL model at imaginary chemical potential. The plot shows the chiral condensate as a function of the temperature at constant Θ

In figure 4.1 the chiral condensate for different Θ of lattice QCD and our results in the PNJL model at imaginary chemical potentials were placed next to each other. Both results show a qualitatively similar behaviour. They both show a smooth crossover transition. However, the absolute values are quite different. The transition in lattice QCD occurs at clearly lower temperatures and also the absolute values of the chiral condensate differ. It should be noted, that $\mu_B = 3\mu$ is the baryo-chemical potential.

In figure 4.2 the chiral susceptibility for lattice QCD and the PNJL model at imaginary chemical potential can be seen. Here, also, the qualitative behaviour is the same. Both

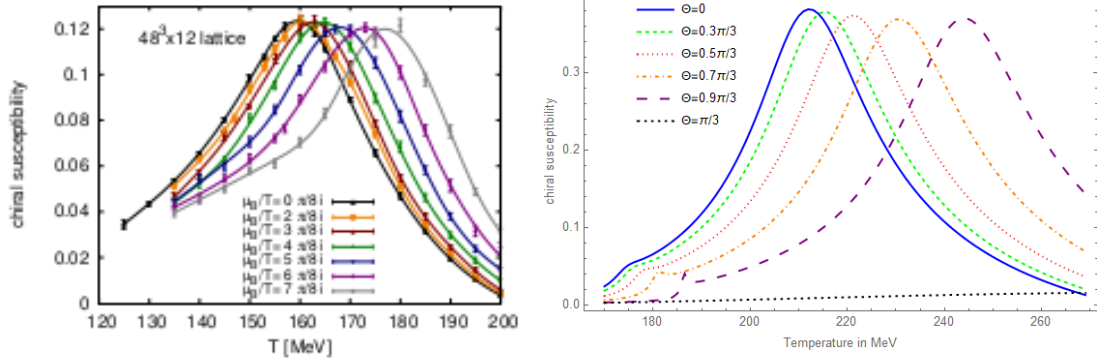


Figure 4.2: Comparison between QCD lattice results (left, taken from [3]) and calculations in the PNJL model at imaginary chemical potential. The plots show the chiral susceptibility as a function of T at constant Θ

results show a peak at the respective transition temperature. The height for all peaks is roughly the same and the peaks are shifted towards higher temperatures, the closer Θ gets to the Roberge Weiss transition at $\Theta = \frac{\pi}{3}$. Again, the absolute peak positions and absolute peak heights are different.

In figure 4.3 the chiral susceptibilities in dependence of the chiral condensate is presented for lattice QCD and the PNJL-model are presented. In both cases the curves are independent from Θ and all curves in both lattice QCD and the PNJL model almost line up. Also, the form of the curves in both models is quite similar. Again, as expected, the absolute values are different.

In [3] the phase transition line was also extrapolated from QCD lattice results to real potential. This has been done by calculating the coefficients κ_2 and κ_4 as well as the transition temperature T_0 . The extrapolated transition line has then the form

$$\frac{T_c(\mu_B)}{T_c(\mu_B = 0)} = 1 - \kappa_2 \left(\frac{\mu}{T_c(\mu_B)} \right)^2 - \kappa_4 \left(\frac{\mu_B}{T_c(\mu_B)} \right)^4. \quad (4.1)$$

The coefficients from [3] are

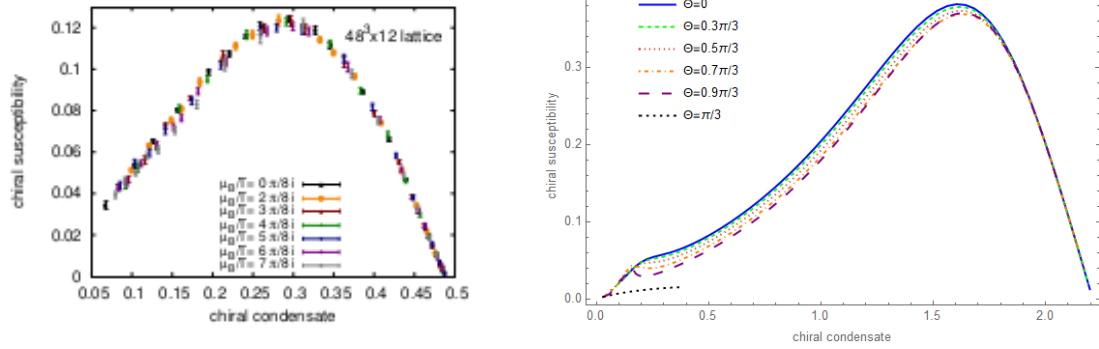


Figure 4.3: Comparison between QCD lattice results (left, taken from [3]) and calculations in the PNJL model at imaginary chemical potentials. The plots show the chiral susceptibilities as a function of the chiral condensate at constant Θ

$$T_0 = 158.0(6) \text{ MeV} \quad \kappa_2 = 0.0153(18) \quad \kappa_4 = 0.00032(67). \quad (4.2)$$

The extrapolated transition line is compared to the transition lines in the PNJL model in figure 4.4. It can be seen, that the crossover transition takes place at significant lower temperatures. It may be, that those results can also be achieved in the PNJL model by varying the fit parameters of the PNJL model, such as T_0 . However, the qualitative behaviour of the PNJL model seems to fit the results of lattice QCD very well.

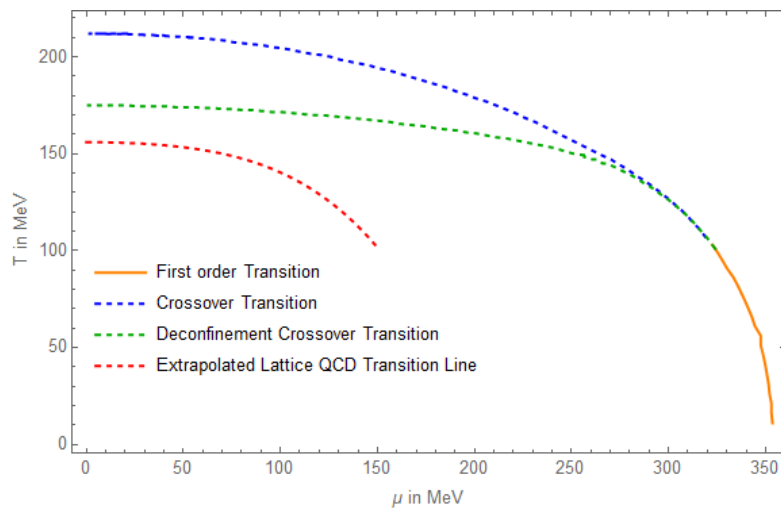


Figure 4.4: The phase diagram of the PNJL model at real chemical potential compared with Lattice QCD results from [3]. The red line denotes the chiral phase transition line extrapolated from lattice QCD results. The respective chiral phase transition in the PNJL model is presented as the blue dashed line.

5 Conclusion and Outlook

In this work the phase transitions of the NJL and the PNJL model were investigated at real and imaginary chemical potential. For that, the respective gap equations were solved and the solution, which minimizes the thermodynamical potential was chosen. The constituent quark mass was taken as order parameter for the chiral phase transition while the expectation value of the Polyakov loop was chosen as order parameter for the confinement/deconfinement transition. Further, a peak in the chiral susceptibility was chosen as crossover criterion for the chiral phase transition.

In both models the phase diagram shows a first order chiral phase transition at low temperatures and high chemical potentials. This then turns into a smooth crossover at higher temperatures. A critical point was also found and calculated. In the PNJL model there was also found a deconfinement phase transition. This takes place as a crossover at lower temperatures than the chiral phase transition. It then joins with the chiral first order phase transition in the vicinity of the critical point.

At imaginary potential the NJL model showed a chiral crossover and a periodicity of 2π with respect to $\Theta = \frac{\mu}{T}$. The PNJL model showed the Roberge Weiss periodicity of $\frac{2\pi}{3}$ and a discontinuity of the order parameters at $\Theta = \frac{\pi}{3}$. This was characterized as the Roberge Weiss first order phase transition. It was also shown, that the chiral susceptibilities at imaginary chemical potential are almost independent of Θ . This was also the case in lattice QCD results from [3].

Furthermore, the results for the PNJL model at imaginary potential were compared with the results of lattice QCD. It was found, that the PNJL model shows the same qualitative behaviour of the chiral condensate and the chiral susceptibility. However, the absolute values for the considered parameters were different. The crossover in lattice QCD for example took place at considerably lower temperatures. Also, the extrapolated chiral

phase transition line was at clearly lower temperatures. The parameters from this work were taken from the literature ([4],[17]). As an outlook, the parameters of the PNJL model can be determined to match the transition lines of lattice QCD. Furthermore, more parts of the phase diagram can be considered, i.e. the color superconductor phase. Also, more flavors could be considered.

Bibliography

- [1] Walter Greiner, Stefan Schramm, and Eckart Stein. *Quantum Chromodynamics*. New York: Springer-Verlag, (1983).
- [2] Michael Buballa. “NJL model analysis of quark matter at large density”. In: *Phys. Rept.* 407 (2005), pp. 205–376. doi: 10.1016/j.physrep.2004.11.004. arXiv: hep-ph/0402234.
- [3] Szabolcs Borsanyi et al. “QCD Crossover at Finite Chemical Potential from Lattice Simulations”. In: *Phys. Rev. Lett.* 125.5 (2020), p. 052001. doi: 10.1103/PhysRevLett.125.052001. arXiv: 2002.02821 [hep-lat].
- [4] Tobias Schulz. *Phasenübergänge im PNJL-Modell bei imaginärem chemischen Potential*. URL: <https://theorie.ikp.physik.tu-darmstadt.de/nhq/downloads/thesis/bachelor.schulz.pdf>.
- [5] J. S. Yndurain. *Quantum Chromodynamics*. New York: Springer-Verlag, (1983).
- [6] P. Schmueser. *Feynman-Graphen und Eichtheorien für Experimentalphysiker*. Berlin-Heidelberg: Springer-Verlag, (1988).
- [7] S. Sarkar and H. Satz. *The Physics of the Quark-Gluon Plasma*. Berlin-Heidelberg: Springer, (2010).
- [8] M. A. Stephanov. “QCD phase diagram: An Overview”. In: *PoS LAT2006* (2006). Ed. by Tom Blum et al., p. 024. doi: 10.22323/1.032.0024. arXiv: hep-lat/0701002.
- [9] Y. Nambu and G. Jona-Lasinio. *Dynamical Model of Elementary Particles Based on an Analogy with Superconductivity*. I. *Phys. Rev.*, 122:345. 1961.
- [10] Daniel Müller. *Untersuchung des Sigma Mesons im NJL Modell am kritischen Punkt des QCD Phasendiagramms*. Bachelor Thesis, Fachbereich Physik, TU Darmstadt. URL: <https://theorie.ikp.physik.tu-darmstadt.de/nhq/downloads/thesis/bachelor.mueller.pdf>.

-
-
- [11] Daniel Müller. *Der Quarkpropagator in selbstkonsistenter $1/N_c$ Entwicklung im NJL Modell*. Master Thesis, Fachbereich Physik, TU Darmstadt. URL: <http://theorie.ikp.physik.tu-darmstadt.de/nhq/downloads/thesis/master.mueller.pdf>.
- [12] J.I. Kapusta and C. Gale. *Finite-Temperature Field Theory. Principles and Applications*. Cambridge University Press, 2006.
- [13] Kenji Fukushima. “Chiral effective model with the Polyakov loop”. In: *Phys. Lett. B* 591 (2004), pp. 277–284. DOI: 10.1016/j.physletb.2004.04.027. arXiv: hep-ph/0310121.
- [14] C. Sasaki, B. Friman, and K. Redlich. “Susceptibilities and the Phase Structure of a Chiral Model with Polyakov Loops”. In: *Phys. Rev. D* 75 (2007), p. 074013. DOI: 10.1103/PhysRevD.75.074013. arXiv: hep-ph/0611147.
- [15] Yuji Sakai et al. “Polyakov loop extended NJL model with imaginary chemical potential”. In: *Phys. Rev. D* 77 (2008), p. 051901. DOI: 10.1103/PhysRevD.77.051901. arXiv: 0801.0034 [hep-ph].
- [16] Kieran Holland and Uwe-Jens Wiese. “The Center symmetry and its spontaneous breakdown at high temperatures”. In: (Nov. 2000). Ed. by M. Shifman and Boris Ioffe, pp. 1909–1944. DOI: 10.1142/9789812810458_0040. arXiv: hep-ph/0011193.
- [17] Simon Roessner, Claudia Ratti, and W. Weise. “Polyakov loop, diquarks and the two-flavour phase diagram”. In: *Phys. Rev. D* 75 (2007), p. 034007. DOI: 10.1103/PhysRevD.75.034007. arXiv: hep-ph/0609281.
- [18] David Scheffler. *The PNJL model at imaginary chemical potential*. Master Thesis, Fachbereich Physik, TU Darmstadt, 2010. URL: <http://theorie.ikp.physik.tu-darmstadt.de/nhq/downloads/thesis/master.scheffler.pdf>.
- [19] Bernd-Jochen Schaefer, Jan M. Pawłowski, and Jochen Wambach. “The Phase Structure of the Polyakov–Quark–Meson Model”. In: *Phys. Rev. D* 76 (2007), p. 074023. DOI: 10.1103/PhysRevD.76.074023. arXiv: 0704.3234 [hep-ph].

6 Appendix

Appendix A

The gap equations of the NJL model at imaginary chemical potential

At imaginary chemical potential, the gap equation yields

$$\begin{aligned} \frac{\partial \Omega}{\partial M} = & \frac{M - m}{2g} - \frac{N_f N_c}{\pi^2} \int_0^\Lambda dp p^2 \frac{M}{E} \\ & + \frac{N_f N_c}{\pi^2} \int_0^\infty dp p^2 \frac{M}{E} \frac{2 \cos(\Theta) e^{-E(p)/T} + 2e^{-2E(p)/T}}{1 + 2 \cos(\Theta) e^{-E(p)/T} + 2e^{-2E(p)/T}}. \end{aligned} \quad (6.1)$$

Susceptibilities in the NJL model

To calculate the susceptibility χ_m , we must calculate $\frac{\partial M}{\partial m}$. This can be done, if we write equation (1.29) as

$$m = M - 8N_c N_f g M \int \frac{d^3 p}{(2\pi)^3} \frac{1}{2E(p)} \left(1 - \frac{1}{1 + e^{(E(p)-\mu)/T}} - \frac{1}{1 + e^{(E(p)+\mu)/T}} \right) \quad (6.2)$$

then the derivative can be written as

$$\begin{aligned} \frac{\partial M}{\partial m} = \left(\frac{\partial m}{\partial M} \right)^{-1} = & \left(1 - 2g \frac{N_f N_c}{\pi^2} \left(\int_0^\Lambda dp \frac{p^2}{E(p)} \left(1 - \frac{M^2}{E(p)^2} \right) \right. \right. \\ & + \int_0^\infty dp \frac{p^2}{E(p)} \left(1 - \frac{M^2}{E(p)^2} \right) (n_q + n_{\bar{q}}) \\ & \left. \left. - \frac{p^2 M}{E(p)^2} \left(\frac{e^{(E(p)-\mu)/T}}{(1 + e^{(E(p)-\mu)/T})^2} + \frac{e^{(E(p)+\mu)/T}}{(1 + e^{(E(p)+\mu)/T})^2} \right) \right) \right)^{-1}. \end{aligned} \quad (6.3)$$

Replacing this in equation (1.53) yields the chiral susceptibility.

Appendix B

Lagrangian of the PNJL model in mean-field approximation

For evaluating the PNJL Lagrangian (1.63), one must evaluate the trace

$$\text{Tr}_c \ln \left(1 + L e^{-E(p)/T} \right). \quad (6.4)$$

with the diagonal form of L

$$L = \text{diag}(e^{i\beta\phi_a}, e^{i\beta\phi_b}, e^{i\beta\phi_c}) \quad (6.5)$$

with

$$\phi_a = \phi_3 + \frac{\phi_8}{\sqrt{3}} \quad \phi_b = -\phi_3 + \frac{\phi_8}{\sqrt{3}} \quad \phi_c = -\frac{2\phi_8}{\sqrt{3}}. \quad (6.6)$$

This yields for the trace

$$\begin{aligned}
\text{Tr}_c \ln\left(1 + L e^{-E(p)/T}\right) &= \ln\left(1 + e^{i\beta\phi_a}\right) + \ln\left(1 + e^{i\beta\phi_b}\right) + \ln\left(1 + e^{i\beta\phi_c}\right). \\
&= \ln\left(1 + (e^{i\beta\phi_a} + e^{i\beta\phi_b} + e^{i\beta\phi_c})e^{-E(p)/T}\right) \\
&\quad + (e^{i\beta(\phi_a+\phi_b)} + e^{i\beta(\phi_b+\phi_c)} + e^{i\beta(\phi_c+\phi_a)})e^{-2E(p)/T} \\
&\quad + e^{i\beta(\phi_a+\phi_b+\phi_c)}e^{-3E(p)/T}.
\end{aligned} \tag{6.7}$$

Using further, that

$$\text{Tr } L = e^{i\beta\phi_a} + e^{i\beta\phi_b} + e^{i\beta\phi_c} = 3\Phi \quad \text{and} \quad \text{Tr } L^\dagger = e^{-i\beta\phi_a} + e^{-i\beta\phi_b} + e^{-i\beta\phi_c} = 3\bar{\Phi} \tag{6.8}$$

yields the PNJL Lagrangian in mean-field approximation (1.64).

The gap equations for the PNJL model

For the PNJL model, the gap equations can be written as

$$\begin{aligned}
\frac{\partial\Omega}{\partial\sigma} &= 2g\sigma - \frac{N_f N_c}{\pi^2} \int_0^\Lambda dp p^2 \frac{m - 2g\sigma}{E(p)} - \frac{N_f}{\pi^2} \int_0^\infty dp p^2 \frac{m - 2g\sigma}{E(p)} \\
&\quad \left(\frac{3\Phi e^{-E(-)/T} + 6\bar{\Phi} e^{-2E(-)} + 3e^{-3E(-)/T}}{g^{(-)}(\Phi, \bar{\Phi}, \sigma)} \right. \\
&\quad \left. + \frac{3\bar{\Phi} e^{-E(+)/T} + 6\Phi e^{-2E(+)} + 3e^{-3E(+)/T}}{g^{(+)}(\Phi, \bar{\Phi}, \sigma)} \right) = 0,
\end{aligned} \tag{6.9}$$

$$\begin{aligned}
\frac{\partial\Omega}{\partial\Phi} &= -\frac{N_f}{\pi^2} \int_0^\infty dp p^2 \left(\frac{3e^{-E(-)/T}}{g^{(-)}(\Phi, \bar{\Phi}, \sigma)} + \frac{3e^{-2E(+)/T}}{g^{(+)}(\Phi, \bar{\Phi}, \sigma)} \right) \\
&\quad - \frac{a(T)}{2} T^4 \bar{\Phi} + b(T) T^4 \frac{-6\bar{\Phi} + 12\Phi^2 - 6\Phi\bar{\Phi}^2}{u_0(\Phi, \bar{\Phi})} = 0,
\end{aligned} \tag{6.10}$$

and

$$\begin{aligned}
\frac{\partial\Omega}{\partial\bar{\Phi}} &= -\frac{N_f}{\pi^2} \int_0^\infty dp p^2 \left(\frac{3e^{-2E(-)/T}}{g^{(-)}(\Phi, \bar{\Phi}, \sigma)} - \frac{3e^{-E(+)/T}}{g^{(+)}(\Phi, \bar{\Phi}, \sigma)} \right) \\
&\quad - \frac{a(T)}{2} T^4 \Phi + b(T) T^4 \frac{-6\Phi + 12\bar{\Phi}^2 - 6\Phi^2\bar{\Phi}}{u_0(\Phi, \bar{\Phi})} = 0.
\end{aligned} \tag{6.11}$$

We used the following relations.

$$\begin{aligned}
E(p) &= \sqrt{p^2 + (-2p\sigma + m)^2}, \\
E(\pm) &= E(p) \pm \mu \\
g^{(-)}(\Phi, \bar{\Phi}, \sigma) &= 1 + 3\Phi e^{-E^{(-)}/T} + 3\bar{\Phi} e^{-2E^{(-)}/T} + e^{-3E^{(-)}/T} \\
g^{(+)}(\Phi, \bar{\Phi}, \sigma) &= 1 + 3\bar{\Phi} e^{-E^{(+)}/T} + 3\Phi e^{-2E^{(+)}/T} + e^{-3E^{(+)}/T} \\
u_0(\Phi, \bar{\Phi}) &= 1 - 6\Phi\bar{\Phi} + 4(\Phi^3 + \bar{\Phi}^3) - 3(\Phi\bar{\Phi})^2
\end{aligned} \tag{6.12}$$

The gap equations for the PNJL model at imaginary potential

At imaginary chemical potential, the gap equations in the PNJL model can be written as

$$\begin{aligned}
\frac{\partial\Omega}{\partial\sigma} &= 2g\sigma - \frac{N_f N_c}{\pi^2} \int_0^\Lambda dp p^2 \frac{m - 2g\sigma}{E(p)} \\
&+ \frac{N_f}{\pi^2} \int_0^\infty dp p^2 \frac{m - 2g\sigma}{E(p)} \frac{6e^{-E(p)/T} + 6|\Psi| \cos(\Theta)(e^{-E(p)/T} + 5e^{-5E(p)/T})}{g_{im}(|\Psi|, \phi, \sigma)} \\
&+ \frac{(9|\Psi|^2 + 6|\Psi| \cos(\phi - 3\Theta))(2e^{-2E(p)/T} + 4e^{-4E(p)/T})}{g_{im}(|\Psi|, \phi, \sigma)} \\
&+ \frac{(54|\Psi|^2 \cos(3\Theta - 3\phi) + 6 \cos(3\Theta))e^{-3E(p)/T}}{g_{im}(|\Psi|, \phi, \sigma)} = 0,
\end{aligned} \tag{6.13}$$

$$\begin{aligned}
\frac{\partial\Omega}{\partial\phi} &= -b(T) \frac{24|\Psi|^3 \sin(3\phi - 3\Theta)}{u_{im}(|\Psi|, \phi, \sigma)} \\
&- \frac{N_f}{\pi^2} \int_0^\infty dp p^2 T \frac{-6|\Psi| \sin(\phi)(e^{-E(p)/T} + e^{-5E(p)/T})}{g_{im}(|\Psi|, \phi, \sigma)} \\
&- \frac{6|\Psi| \sin(\phi - 3\Theta)(e^{-2E(p)/T} + e^{-4E(p)/T})}{g_{im}(|\Psi|, \phi, \sigma)} \\
&+ \frac{54|\Psi|^2 \sin(3\Theta - 3\phi)e^{-3E(p)/T}}{g_{im}(|\Psi|, \phi, \sigma)} = 0,
\end{aligned} \tag{6.14}$$

and

$$\begin{aligned}
\frac{\partial \Omega}{\partial |\Psi|} = & -a(T)T^4 |\Psi| + b(T) \frac{-12|\Psi| + 24|\Psi|^2 \cos(3\phi - 3\Theta) - 12|\Psi|^3}{u_{im}(|\Psi|, \phi, \sigma)} \\
& - \frac{N_f}{\pi^2} \int_0^\infty dp p^2 T \frac{6 \cos(\phi)(e^{-E(p)/T} + e^{-5E(p)/T})}{g_{im}(|\Psi|, \phi, \sigma)} \\
& \frac{18|\Psi| \cos(3\Theta - 3\phi) + 6 \cos(\phi - 3\Theta)(e^{-2E(p)/T} + e^{-4E(p)/T})}{g_{im}(|\Psi|, \phi, \sigma)} \\
& \frac{(36|\Psi| \cos(3\Theta - 3\phi) + 2 \cos(3\Theta))e^{-3E(p)/T}}{g_{im}(|\Psi|, \phi, \sigma)} = 0.
\end{aligned} \tag{6.15}$$

We used the following relations.

$$\begin{aligned}
E(p) &= \sqrt{p^2 + (-2p\sigma + m)^2}, \\
g_{im}(|\Psi|, \phi, \sigma) &= 1 + e^{-6E(p)/T} + 6|\Psi| \cos(\phi)(e^{-E(p)/T} + e^{-5E(p)/T}) \\
&+ (9|\Psi|^2 + 6|\Psi| \cos(\phi - 3\Theta))(e^{-2E(p)/T} + e^{-4E(p)/T}) \\
&+ (18|\Psi|^2 \cos(3\Theta - 3\phi) + 2 \cos(3\Theta))(e^{-3E(p)/T}) \\
u_{im}(|\Psi|, \phi, \sigma) &= 1 - 6|\Psi|^2 + 8|\Psi|^3 \cos(3\phi - 3\Theta) - 3|\Psi|^4.
\end{aligned} \tag{6.16}$$

Acknowledgements

I want to thank particularly my revisor, PD Dr. Buballa for his continuous support during this work. He was always ready to answer my questions.

Furthermore I want to thank my parents for supporting me throughout the time of my studies.